Investigating the Microwave Behaviour of Solid Carbon in Natural Gas Pyrolysis under Microwave Irradiation

by

Sama Manzoor

A thesis submitted in partial fulfillment of the requirements for the degree of

Master of Science
in
Chemical Engineering

Department of Chemical and Materials Engineering
University of Alberta

Abstract

The rising levels of carbon dioxide emissions stemming from the combustion of fossil fuels necessitate immediate attention to implement sustainable energy solutions. Hydrogen as a fuel, holds significant potential for establishing CO_2-neutral systems, and the utilization of microwave pyrolysis of methane is emerging as an innovative and promising approach in this regard. In contrast to conventional hydrogen production methods that generate CO_2 by products, the microwave-driven methane pyrolysis process exclusively yields solid carbon and hydrogen gas as its byproducts. To enhance our understanding of this technique and its scalability, it is essential to explore the microwave characteristics of the carbon used and generated during this process.

This thesis provides fundamental insights into the microwave heating behaviour of solid carbon and how it translates to cracking of methane into hydrogen. We investigated the microwave properties of two carbon samples (seed carbon; SC and product carbon; PC) from microwave-driven pyrolysis of methane. We employed cavity perturbation technique from room temperature to 1250°C across frequencies of 397, 912, 1429, 1948, and 2467 MHz. Thermogravimetric analysis (TGA), differential scanning calorimetry (DSC), and X-ray diffraction (XRD) analysis were conducted for further insight. SC exhibited an initial permittivity decline up to 200°C due to moisture release, confirmed by TGA/DSC showing a 5% mass loss from 100-155°C. Subsequently, permittivity peaked and then decreased due to high conductivity. PC displayed fluctuating permittivities but maintained consistent values. PC, generated at elevated temperatures, showed no moisture loss in TGA/DSC. These findings indicate that the microwaves can penetrate and heat both the samples uniformly across their entire volume, resulting in efficient heating. SC had higher permittivity, making it more responsive to microwaves, but its potential for thermal runaway in microwave-driven pyrolysis applications is a concern. XRD analysis revealed that both

SC and PC had amorphous carbon structures, with PC showing some signs of graphitization. Both carbons can serve as effective microwave heat carriers in methane pyrolysis, potentially eliminating the need for costly catalysts and enabling a self-sufficient process.

While microwave pyrolysis of methane has proven to be effective in producing a substantial quantity of hydrogen, the reactor's fluidization process is of paramount importance. Therefore, the second part of the thesis further reviewed the diverse comminution behaviours observed in fluidized reactors concerning carbon materials. This study is essential for understanding the actual combustion rate, thermal efficiency, and particle size distribution of carbonaceous solids during fluidized bed combustion. Factors such as porosity, particle size, volatile content, and bed temperature heavily influence particle fragmentation.

The outcomes of this thesis will play a significant role in improving the efficiency and efficacy of microwave pyrolysis of methane and its associated applications, thereby advancing the path towards a more sustainable and economically viable energy solution.

Preface

This thesis is an original work conducted by Sama Manzoor under the supervision of Professor Erin Bobicki, containing published contents from the peer-reviewed journals as described below:

Paper 1: Manzoor, S., Wani, O. B., & Bobicki, E. R. (2024). Investigating the microwave properties of carbon materials from microwave-driven methane pyrolysis. Carbon Trends, 100326.

Paper 2: Manzoor, S., Tatum, J., Wani, O. B., & Bobicki, E. R. (2023). Comminution of carbon particles in a fluidized bed reactor: A review. Minerals Engineering, 195, 108026.

Acknowledgments

I extend my heartfelt gratitude and praises to Almighty Allah, the Most Compassionate and the Most Merciful, for bestowing upon me the strength to endure difficult moments and showering me with His mercy and blessing throughout this journey.

I am grateful to my advisor, Professor Erin Bobicki, for her support and for providing me with the invaluable opportunity to embark on this academic endeavor. I would also like to express my gratitude to Professor Thomson and his research group at the University of Toronto for their assistance whenever I sought help. Additionally, I am thankful to all the individuals at MPN, McMaster University, and UNBC who offered their cooperation and support during my work.

I would like to acknowledge the National Sciences and Engineering Research Council of Canada (NSERC) for their financial support and the Faculty of Graduate Studies and Research for honoring me with University of Alberta Graduate Recruitment Scholarship, Captain Thomas Farrell Greenhalgh Memorial Graduate Scholarship and Donald Lougheed Engineering Graduate Scholarship.

I want to offer my sincere appreciation to my research group colleagues, Caroline, Zube, Rebecca, and James, and a very special thanks to Dr. John Forster. Thank you all for your help, moral support, and encouragement throughout my time at U of A. Their readiness to assist whenever needed was truly commendable.

I wish to acknowledge my deepest thanks to the Kashmiri community in Edmonton. Their warmth and sense of family have been a source of comfort and encouragement, especially when being far away from home.

I am indebted to my beloved parents, Dr. Manzoor Ahmad Dar and Dr. Rubina Rashid. I am, and forever will be, grateful for their unconditional love, dedication and support which have been the driving force behind my achievements. Their constant belief in my abilities, endless encouragement, and sacrifices have been instrumental in my accomplishments. I also want to thank my wonderful sisters, Dr. Sehar Manzoor and Serat Manzoor, for their support and understanding during both the challenging and joyful moments of this journey. Their constant presence and motivation have been a source of strength and inspiration.

I am immensely grateful to my dear husband, Dr. Omar Bashir Wani. I express my deepest thanks for his unwavering love, support and for being my pillar of strength. I am truly fortunate to have you by my side. Thank you for being my rock and my biggest supporter. This achievement is as much yours as it is mine.

Lastly, my boundless love goes to my beautiful daughter, Maryam Omar Wani, who entered my life during my academic journey, bringing new perspectives and joys. I hope that my achievements serve as an inspiration for her as she grows.

Table of Contents

List of Tables

List of Figures

List of Abbreviations

CO_2 – Carbon dioxide

CH_4- Methane

CO- Carbon monoxide

H_2- Hydrogen

K- Kelvin

°C- Celsius

g- Gaseous state

s- Solid state

T- Temperature

MHz- Megahertz

GHz- Gigahertz

ω- Radial frequency

$\varepsilon^*_r(\omega)$- Relative complex permittivity

$\varepsilon^*(\omega)$- Complex permittivity

ε_0- Permittivity of free space

$\varepsilon'_r(\omega)$- Relative real permittivity

$\varepsilon'(\omega)$- Real permittivity

$\varepsilon''_r(\omega)$- Relative imaginary permittivity

$\varepsilon''(\omega$- Imaginary permittivity

j- Constant value = $\sqrt{-1}$

tan δ- Loss tangent

D_p- Penetration depth

λ_o- Incident wavelength

π- Pi

SC- Seed carbon

PC- Product carbon

TGA- Thermogravimetric analysis

DSC- Differential scanning calorimetry

XRD- X-ray diffraction

ICPOES- Inductively coupled plasma atomic emission spectroscopy

μm- Micrometer

λ- Wavelength

Å- Angstrom = 10^{-10} m

°- Degree angle

2θ- Angle between transmitted beam and reflected beam

FWHM- Full width at half maximum

La- Lateral size

Lc- Stacking height

βa- Full width at half maximum of fitted 101 peak

βc- Full width at half maximum of fitted 002 peak

%- Percentage

mm- Millimeter

A.U.-Arbitrary unit

nm- Nanometer

kW- Kilo Watts

ID- Internal diameter

O_2- Oxygen

S_f- Fragmentation index

Chapter 1
Introduction and Outline

1.1 Overview

The increase in global population along with rapid urbanization of developing nations has led to a rise in energy demand. Fossil fuels are projected to be the main energy source for the next two decades, this however, will result in increased CO_2 emissions in the atmosphere thereby causing global warming [1]. To meet the goals of the Paris agreement and to prevent a climate catastrophe due to anthropogenic emissions, it is imperative to decarbonize the primary energy sources by transitioning to clean, sustainable and renewable energy. Among the different alternate sources, hydrogen as a clean fuel is a promising substitute to the traditional fossil fuels. Not only does it have the features of a long term clean and safe energy carrier, but it also has highest energy per unit [2]. Hydrogen can be used with high efficiency, and possesses the properties of being versatile, inexhaustible, convenient, and independent from foreign control [3].

Hydrogen can be produced using different technologies, feedstocks, and pathways. The benchmark process to produce hydrogen is steam reforming of methane, followed by water-gas shift reaction to generate more hydrogen. This process ultimately yields a large amount of CO_2 as one of the final products which has a negative impact on the environment [4]. Other conventional methods such as coal gasification, hydrocarbon reforming, water electrolysis, molten metal catalysis and plasma arc tube are too expensive [5].

Our research group has recently developed a novel method for hydrogen production using microwave pyrolysis that involves the removal of CO_2 from the loop, resulting in the formation of solid carbon and hydrogen. This approach shows great promise; however, it is crucial to gain a comprehensive understanding of the microwave properties associated with this carbon material.

By investigating the microwave characteristics, we can further evaluate the potential applications of this carbon and optimize its utilization.

1.2 Objective

The objective of this work was to investigate the microwave properties of the seed carbon used and product carbon generated during microwave-driven pyrolysis of methane.

1.3 Hypothesis

The sole by-product of the methane molecule during microwave pyrolysis is solid carbon material, which is produced in significant quantities. This emphasizes the importance of conducting a thorough examination of this material. Carbon solids posses excellent microwave absorbing properties, thus allowing them to participate in reactions in the form of heating media, or indirectly heat microwave transparent materials. Accurate measurement of microwave properties of carbon such as real and imaginary permittivity, loss tangent and penetration depth are essential for the development of a microwave technology. Knowledge of complex permittivities as a function of temperature and frequency is crucial for comprehending the material behaviour in microwave field, and also to regulate heating behaviour. This information is necessary for scaling up process and designing industrial systems. The hypothesis is that carbon produced during microwave pyrolysis of methane can be used as a microwave carrier which will transfer heat to methane gas, thereby removing the need for expensive catalysts and making the process self sufficient.

1.4 Thesis outline

This thesis has been written in the form of chapters and the structure of this thesis is as follows:

Chapter 1 provides a general overview of the thesis and defines the objectives.

Chapter 2 conducts a literature review on hydrogen as a fuel, exploring various production pathways, explaining the fundamentals of microwave and microwave heating involving carbon.

Chapter 3 presents the findings of microwave heating behaviour of the carbon used and generated during microwave-driven methane pyrolysis.

Chapter 4 presents the review of different comminution processes of carbon materials observed in fluidized bed reactor as used in the microwave methane pyrolysis.

Chapter 5 presents the conclusions and recommendations from this work.

Chapter 2
Literature Review

2.1 Introduction

In recent years, there has been a significant rise in CO_2 emissions, resulting in the greenhouse effect. Approximately 20% of the global thermal absorption can be attributed to CO_2 alone. The burning of fossil fuels is the main cause of this anthropogenic gas and is responsible for the largest share of greenhouse gas emissions [6]. Over the past 50 years, CO_2 emissions have accounted for approximately 80% in the US and 87% in Canada [7]. The increasing global population is driving up the demand for energy, which in turn will lead to a higher production of CO_2 since fossil fuels are expected to remain the primary energy source for the next two decades. Hence, there is an urgent need to develop an energy source that is CO_2 neutral [1].

Hydrogen is a promising substitute to the traditional fossil fuels. It offers the advantages of being a long-term, clean, and secure energy carrier, while also having the highest energy density per unit [8]. Additionally, hydrogen exhibits high efficiency in its utilization and possesses versatile qualities, being both abundant and convenient, while also being independent of foreign control [3]. One of the significant benefits of hydrogen is its potential to significantly decrease CO_2 emissions and minimize other pollutants that arise from the combustion of fossil fuels [9].

2.2 Hydrogen production methods

The primary method for hydrogen production involves the steam reforming of methane, followed by the water-gas shift reaction, which generates additional hydrogen. Unfortunately, this process results in the production of a significant amount of CO_2 as one of the end products [10]. Additionally, the hydrogen produced through this process requires further purification, leading to the presence of substantial amounts of CO_2 in the stream [11].

Other conventional techniques for hydrogen productions are either considered costly as in coal gasification, water electrolysis, molten metal catalysis, and plasma arc tube [1] or generate low hydrogen quantity [12]. Catalytic pyrolysis of methane is yet another method, however, it has a major disadvantage as the catalyst used is deactivated by carbon surface deposits [13].

Recently, a novel method called microwave pyrolysis of methane has emerged as an innovative approach that serves two objectives simultaneously: the production of clean hydrogen fuel and the capture of carbon that would otherwise be released as CO_2 during combustion [14]. This method entails exposing natural gas to microwave radiation and utilizing microwave carriers, such as carbon, to facilitate heat transfer to the gas [15]. Consequently, the process yields gaseous hydrogen and solid carbon as products.

The following section gives an overview of various methods used for hydrogen production, with a concise summary provided in Table 2.1.

Table 2.1. Hydrogen generation technologies. Reproduced from [2].

Production Method	**Feedstock**	**Efficiency**	**Maturity**
Steam reforming	Hydrocarbons	70-85%	Commercial
Partial oxidation	Hydrocarbons	60-75%	Commercial
Autothermal reforming	Hydrocarbons	60-75%	Near term
Plasma reforming	Hydrocarbons	9-85%*	Long term
Biomass gasification	Biomass	35-50%	Commercial
Aqueous phase reforming	Carbohydrates	35-55%	Medium term
Electrolysis	H_2O + electricity	50-70%	Commercial
Photolysis	H_2O + sunlight	0.5%*	Long term
Thermochemical water splitting	H_2O + heat	-	Long term

*Hydrogen purification not included

2.2.1 Steam reforming

Steam reforming of natural gas is a widely adopted method in industries [3], accounting for approximately 40% of hydrogen production [12]. However, this process is associated with the highest air emissions [4]. Figure 2.1 illustrates the key processing steps involved in a steam reforming unit. The process entails two main steps. In the first step, hydrocarbon raw materials are mixed with steam and introduced into a catalytic reactor to generate syngas. To prevent catalyst deactivation, these raw materials must be free of sulphur, which can be achieved through a desulfurization process [2], [3]. The feedstock can include light hydrocarbons like natural gas and naphtha, as well as biogas or methanol [12]. Subsequently, the gas product is directed into a carbon monoxide catalytic converter, where steam transforms CO into carbon dioxide and hydrogen through the water gas shift reaction [2], [3]. Catalysts utilized in this process can be categorized into non-precious metals, such as nickel, or precious metals, like platinum or rhodium-based [4]. The primary reactions occurring during steam reforming of natural gas are represented by the following equations [3]:

$$CH_4 + H_2O \leftrightarrow CO + 3H_2 \qquad \Delta H^o{}_{298K} = 206.4\ kJ/mol \qquad \textbf{(2.1)}$$

$$C_nH_{2n+2} + nH_2O \rightarrow nCO + (2n+1)H_2 \qquad \Delta H^o{}_{298K} > 0 \qquad \textbf{(2.2)}$$

$$CO + H_2O \leftrightarrow CO_2 + H_2 \qquad \Delta H^o{}_{298K} = -41.2\ kJ/mol \qquad \textbf{(2.3)}$$

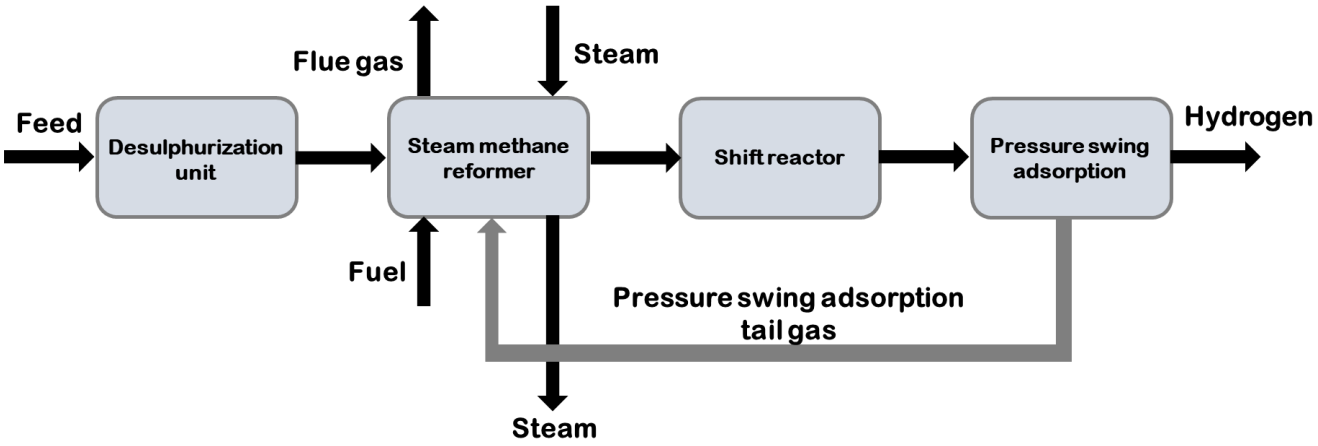

Figure 2. 1. Steam Reforming Plan Diagram. Adapted from [12].

2.2.2 Partial oxidation

Partial oxidation is a non-catalytic process that involves the gasification of raw materials using oxygen in an exothermic reaction, eliminating the need for external heat [2], [3]. This process yields hydrogen at a higher rate than steam methane reforming, but with a lower overall hydrogen output [12]. The most commonly used feedstocks for partial oxidation are heavy residual oils or coal. When the fuel is combined with oxygen, it undergoes conversion into H_2, CO, and CO_2, as illustrated in Figure 2.2. The primary steps of this process include gasification, cooling and cleaning of syngas, shifting of syngas, and ultimately the purification of hydrogen [12]. To reduce processing temperatures, catalysts can be introduced in a process known as catalytic partial oxidation. This reaction occurs within a temperature range of 1300–1500°C and a pressure range of 3–8 MPa, ensuring complete conversion and minimizing carbon or soot formation [4].

The equation for partial oxidation is as following [5]:

$$CH_4 + \frac{1}{2}O_2 \rightarrow 2H_2 + CO \qquad \Delta H^o{}_{298K} = -43.6\ kJ/mol \qquad \textbf{(2.4)}$$

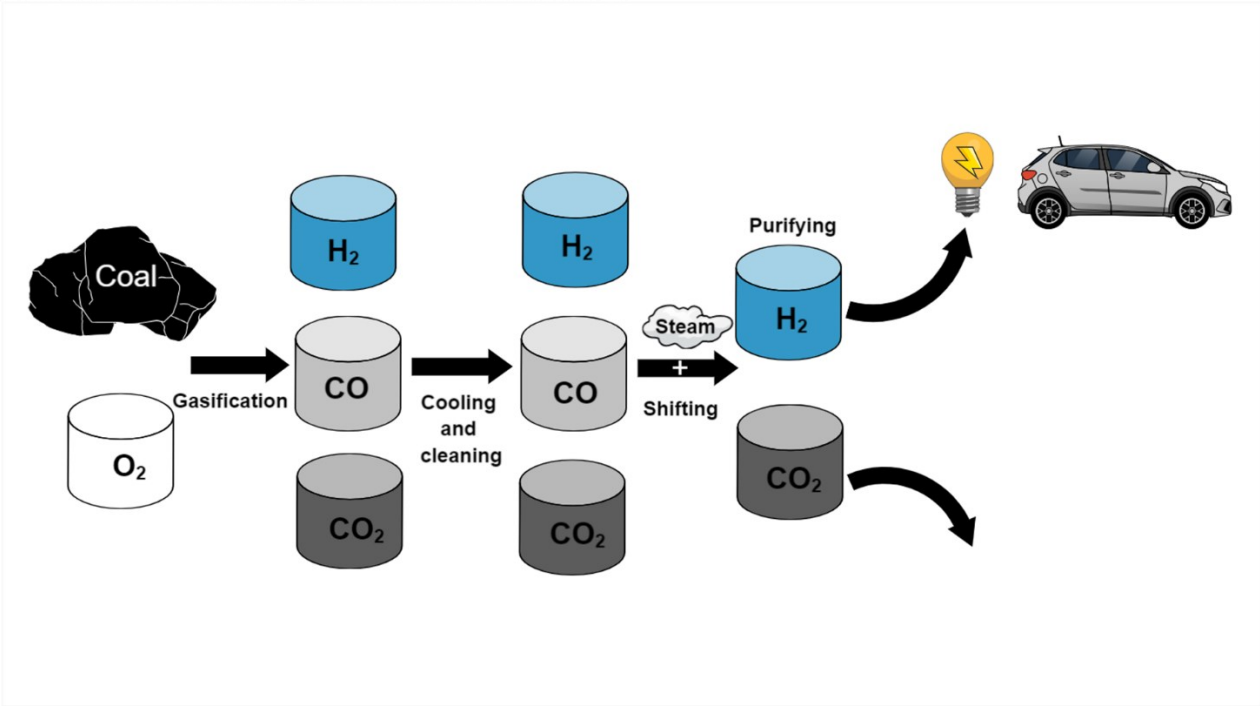

Figure 2. 2. Partial Oxidation Process. Adapted from [12].

2.2.3 Autothermal reforming

Autothermal reforming is a process that combines the steps of partial oxidation or catalytic partial oxidation with the addition of steam. This addition of steam supplies the necessary heat to drive the reforming process [3], [4]. By combining both steam reforming (endothermic) and partial oxidation (exothermic) processes, this method becomes self-sustaining and does not require any external heat. As a result, autothermal reforming is simpler and more cost-effective compared to traditional steam reforming of methane [2].

2.2.4 Plasma reforming

Plasma reforming shares similar overall reactions with conventional reforming. However, in this process, plasma serves as the source of energy and generates free radicals through heat or electricity. Injecting steam into the fuel leads to the creation of radicals and electrons, creating conditions for reductive and oxidative reactions to occur [2]. Compared to conventional reforming,

plasma reforming offers numerous advantages, including lower costs, reduced catalyst deterioration, fewer limitations on hydrogen production from heavy hydrocarbons, and the ability to operate at lower temperatures [4].

2.2.5 Conventional pyrolysis

In pyrolysis of methane, hydrogen and carbon are produced in the absence of oxygen. Carbon monoxide and carbon dioxide are not formed, hence, there is no need for secondary reactions like water gas shift or partial oxidation. This method also results in lesser emissions as solid carbon and hydrogen are the only two products. Fuel flexibility, simplicity and compactness, and clean carbon by-products are some of the advantages of this process [2]. Methane pyrolysis has been categorized into 3 main groups namely, thermal decomposition, plasma decomposition and catalytic decomposition [16], as shown in Figure 2.3.

The following reaction takes place in methane pyrolysis:

$$CH_4(g) \rightarrow 2H_2(g) + C(s) \quad \textbf{(2.5)}$$

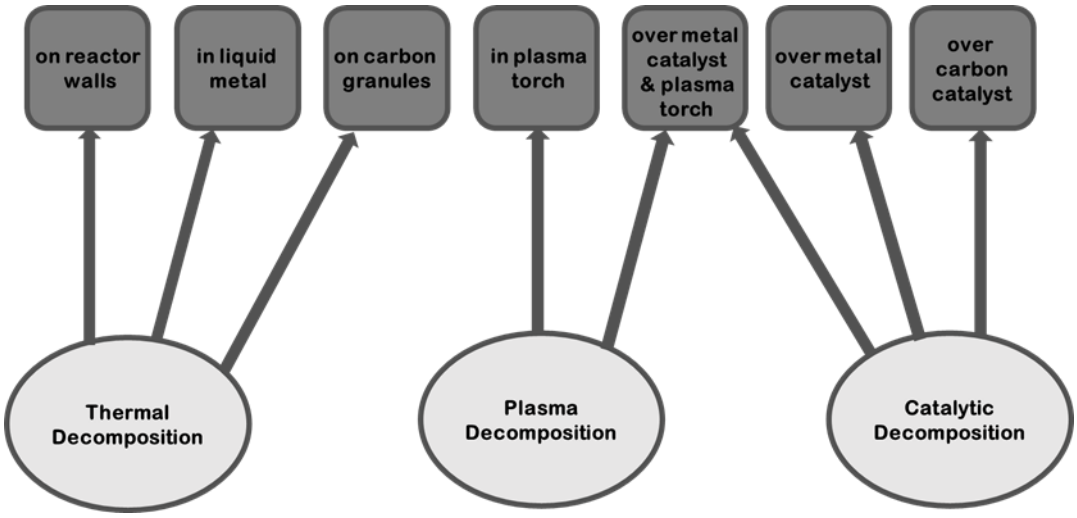

Figure 2. 3. Methane decomposition methods. Adapted with permission from [16]. Copyright 2020 John Wiley and Sons.

Thermal decomposition of methane demands reaction temperatures above 1000°C [17]. When process heat is supplied through the reactor walls, it causes soot deposition on hot surfaces, leading to operational disruptions and heat transfer decline [16], [18].

Plasma decomposition utilizes a plasma torch to generate high local energy densities and temperatures, reaching up to 2000°C. The actual plasma torch faces significant technical limitations, including cooling, electrode wear, and carbon deposits [16].

Catalytic decomposition usually exhibits favourable reaction and conversion rates even at temperatures below 1000°C [16]. However, it has a major drawback as the catalyst used becomes deactivated due to carbon surface deposits, necessitating the burning off of these deposits to restore the catalyst's original activity. This regeneration process generates CO_2 as a by-product [19].

2.2.6 Microwave pyrolysis

Microwave pyrolysis of methane converts natural gas directly into hydrogen and solid carbon, thus, there is no need for carbon capture and storage. This process is also environmentally friendly as there are zero carbon emissions [15]. Additionally, this process does not require the use of high alloy reactor materials, expensive catalysts, and desulfurization of the feedstock [20]. Assuming cheap natural gas accessibility, this method has the potential to produce hydrogen at a reasonable cost [16]. Therefore, it results in not only less pollution but also gives higher efficiencies [21]. Studies have shown that microwave-assisted pyrolysis of methane shows greater conversion rates when microwave power was increased, and when methane flow was reduced [20]. Furthermore, methane conversions are more significant compared to conventional heating at temperatures less than or equal to 800°C [22].

Numerous studies have been conducted investigating the use of microwave plasmas for methane pyrolysis, with a specific emphasis on nanocarbon production [23], [24], [25], [26], [27]. Juda et al. attained a 90% conversion rate without a catalyst, but needed significant amounts of nitrogen to stabilize the plasma, leading to a diluted product stream [23]. On the other hand, Medvedev et al., utilized a Ni catalyst bed and achieved a conversion rate of 40–80%. However, the formation of solid carbon destabilized the microwave torch [24], [25], [26], [27].

In another study, Zeng et al. conducted microwave pyrolysis of methane at temperatures between 1300 K and 1400 K to produce carbon nanospheres and carbon nanotubes in absence of a catalyst. Although hydrogen production was not mentioned, it is worth noting that they employed a commercial carbon composite as a microwave susceptor [28].

In other literature, catalytic properties of carbon materials were employed to facilitate the microwave decomposition of methane at lower temperatures. However, the presence of the carbon

product resulted in the deactivation of the catalyst, blockage of the packed-bed reactors, and a considerable decrease in methane conversion over time [20], [22].

Recently, a new technique to produce hydrogen via microwave-induced methane pyrolysis has emerged [15]. This technology, as shown in Figure 2.4, involves subjecting natural gas to microwave radiation. This process entails exposing activated carbon (known as seed carbon; SC) to microwaves, serving as a microwave receptor to heat methane gas up to temperatures of 1200°C and convert it into pure hydrogen gas and solid carbon. The resulting product carbon (PC) could function as a microwave receptor, sustaining the methane pyrolysis process.

Microwave pyrolysis of methane has demonstrated its ability to yield a high amount of hydrogen, but the fluidization process is crucial within the reactor [15]. During fluidization, carbon particles inside the reactor undergo comminution, a process of breaking down or reducing particle size. The diverse comminution behaviours observed in fluidized reactors concerning carbon materials have been comprehensively summarized in a review paper presented as chapter 4 of this thesis.

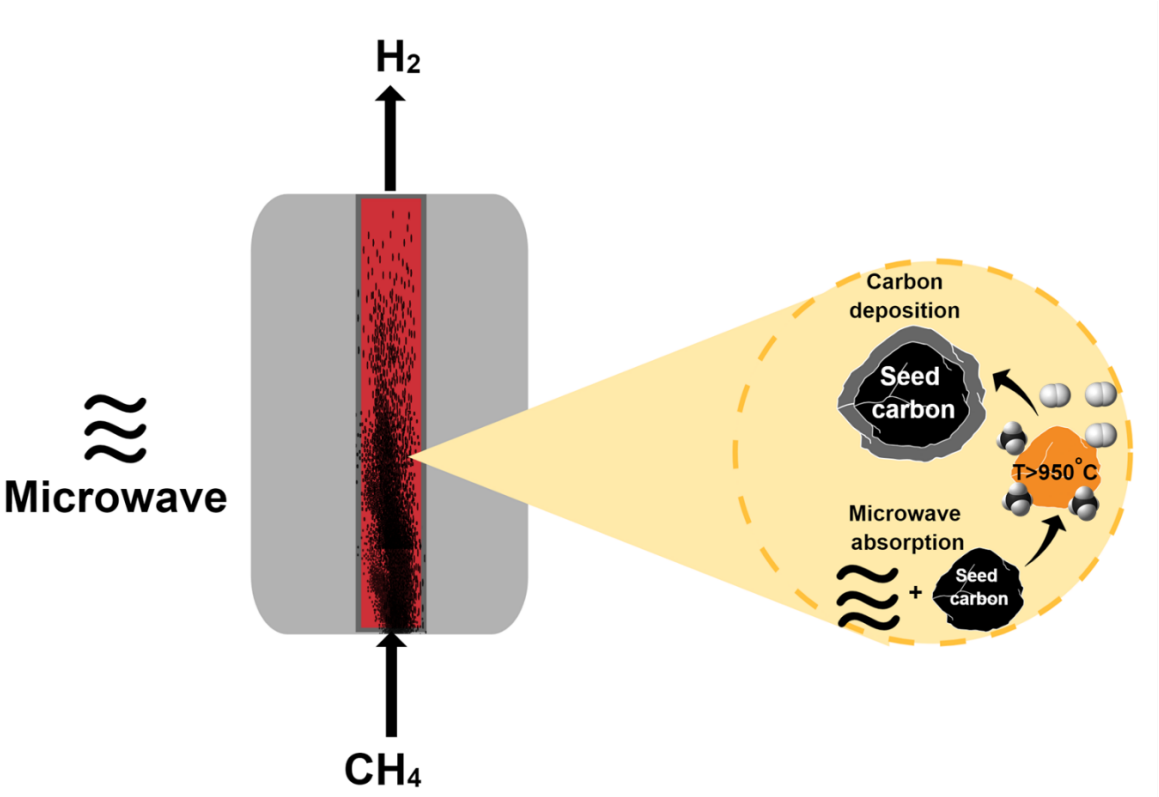

Figure 2. 4. Schematic diagram depicting microwave-driven methane pyrolysis. Adapted with permission from [15]. Copyright 2023 Elsevier.

2.3 Fundamentals of Microwave Heating

Microwaves, as a form of electromagnetic radiation, encompass a wide frequency range between 300 MHz to 300 GHz, occupying the spectrum between infrared and radio frequencies [29]. In North America, specific frequencies have been approved for microwave applications, with 915 MHz designated for industrial use and 2450 MHz for domestic purposes [30]. Microwave heating has several advantages over conventional heating such as faster heating rate, selective non-contact heating, direct volumetric heating, clean energy source, uniform heating, quick start up and shut down, easy automation, and cost efficiency [29], [30], [31], [32]. Such benefits of microwaves have enabled them to be applied in different technological and scientific fields [32].

Microwave heating of materials stands apart from conventional heating methods due to the fundamental distinction in the heat transfer mechanism, as depicted in Figure 2.5. Conventional heating relies on heat transfer through conduction, convection, and radiation, with heat moving from the hotter external surface to the cooler core region of the material. Conversely, microwave heating operates by directly absorbing electromagnetic energy within the material, leading to heat generation from within. As a result, heat transfer occurs from the hotter internal region to the cooler outer surfaces of the material during microwave heating processes [33].

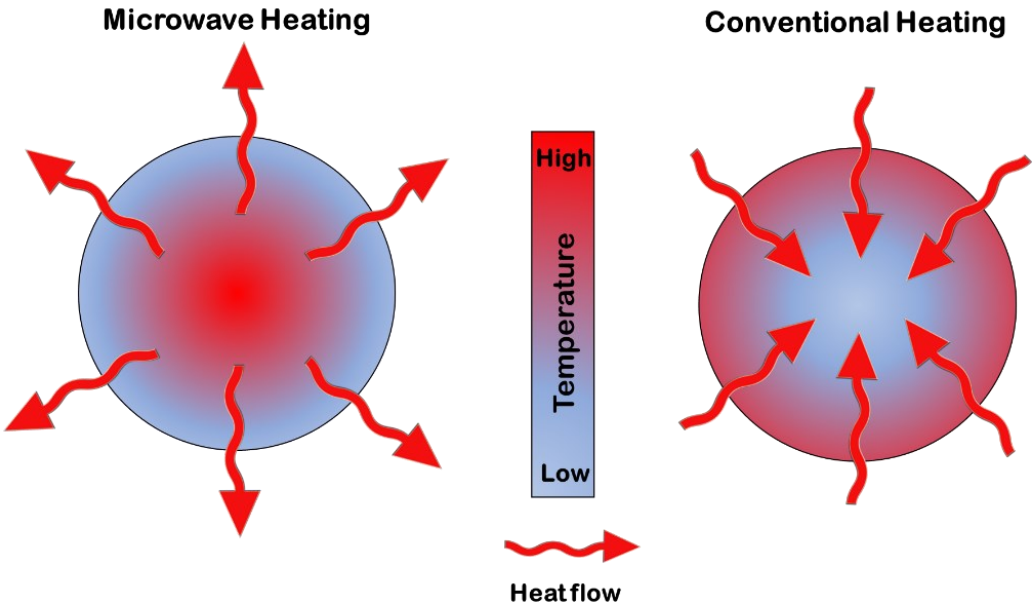

Figure 2. 5. Illustration of temperature gradient and heat transfer from microwave and conventional heating methods. Adapted with permission from [31]. Copyright 2023 Royal Society of Chemistry.

Microwave interaction depends on the nature of material (conductors, insulators and dielectric materials) and degree of interaction [31]. Generally, materials can either reflect, transmit, or absorb microwaves [30], [34]. For instance, metals, being opaque materials, act as excellent reflectors and

are not heated by microwaves as they simply bounce off from their surface [31], [34]. Transparent materials like quartz can transmit microwaves when it passes through them without causing any substantial change due to microwave interaction [34]. On the contrary, materials that can absorb microwaves, such as polar liquids, are referred to as microwave absorbers and can instantly produce heat [31], [32]. They exhibit a diverse range of properties, encompassing both conductive and insulating characteristics. These materials are commonly known as lossy dielectrics or high dielectric loss materials due to their propensity to efficiently absorb electromagnetic energy and convert it into heat [35]. Microwave heating is based on the principle that a material absorbs microwave energy and changes it into heat. Different types of materials and their interactions with microwave radiation is shown in Figure 2.6.

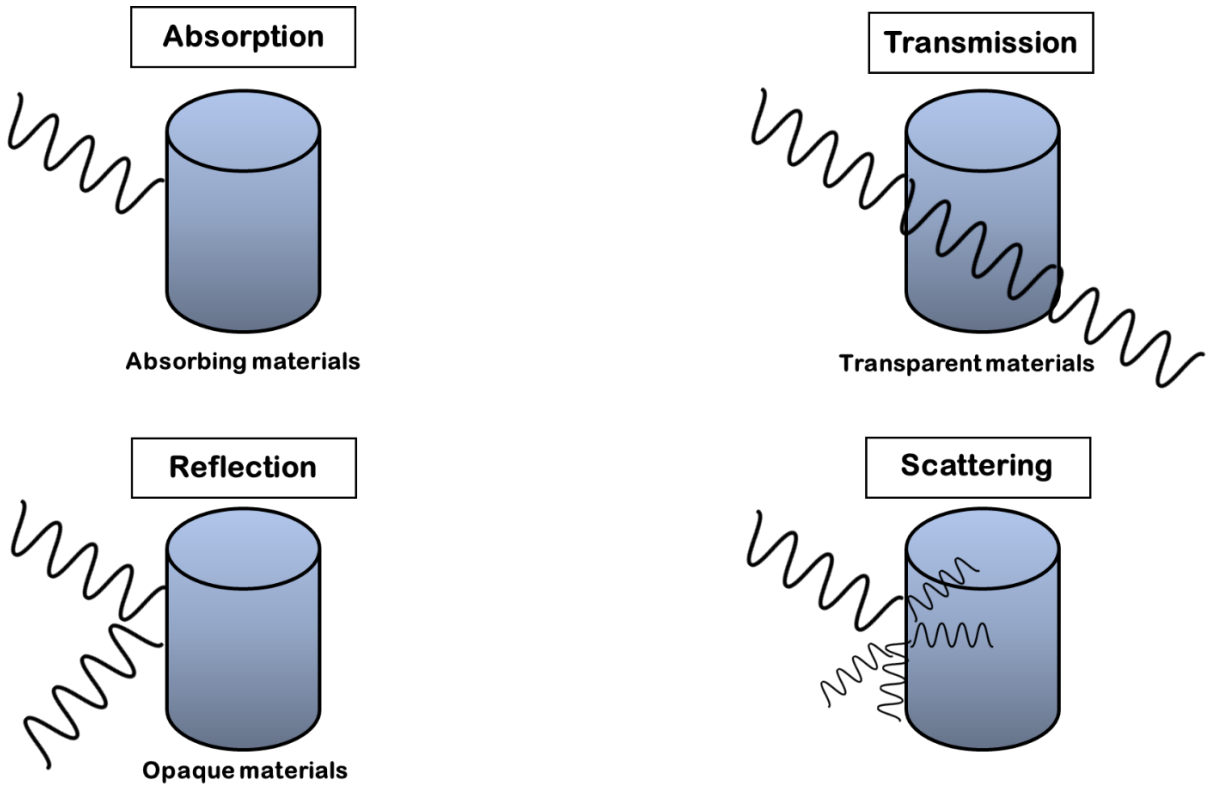

Figure 2. 6. Microwave interaction with different materials. Adapted with permission from [35].

The mechanism of microwave heating differs between solutions and solids [29]. In liquids or solutions, two main interactions take place: dipolar rotation and ionic conduction [34]. In dipolar rotation, the molecules with dipole moments align themselves with the changing microwave field, causing friction and collisions that result in heating [36]. In contrast, ionic conduction involves the movement of ions through the solution, driven by the microwave field, which generates heat [36].

In solids, particularly those electron-rich materials lacking freely movable dipoles (e.g., carbon materials), heating occurs through the motion of electrons via Joule current within the grain or phase boundaries [29], [36]. Unlike liquids, solid materials rely on electron motion for heat generation in response to the microwave field.

2.3.1 Dielectric Polarization

When microwaves interact with a dielectric material, they cause the charged particles within the material to shift from their average equilibrium positions. This phenomenon gives rise to different types of polarization, each characterized by distinct mechanisms (Figure 2.7) [29], [30], [37]:

1. Electronic polarization occurs due to the displacement of electrons around the nuclei of atoms within the dielectric material. As the microwave field interacts with the electrons, they experience a net displacement, leading to polarization effects.

2. Atomic or ionic polarization results from the displacement of atomic nuclei within the dielectric. This displacement arises from the non-uniform distribution of charge during the formation of molecules, causing the atoms to respond to the microwave field.

3. Dipolar or orientation polarization is observed in polar dielectrics containing permanent dipoles. Here, polarization occurs through the reorientation of these dipoles. The microwave field induces alignment changes in the permanent dipoles, leading to polarization of the material.

4. Interfacial or spatial charge (also known as Maxwell-Wagner polarization) arises when free electrons accumulate at the grain or phase boundaries or surfaces of the dielectric material. The microwave field induces the movement of these free electrons, resulting in polarization effects.

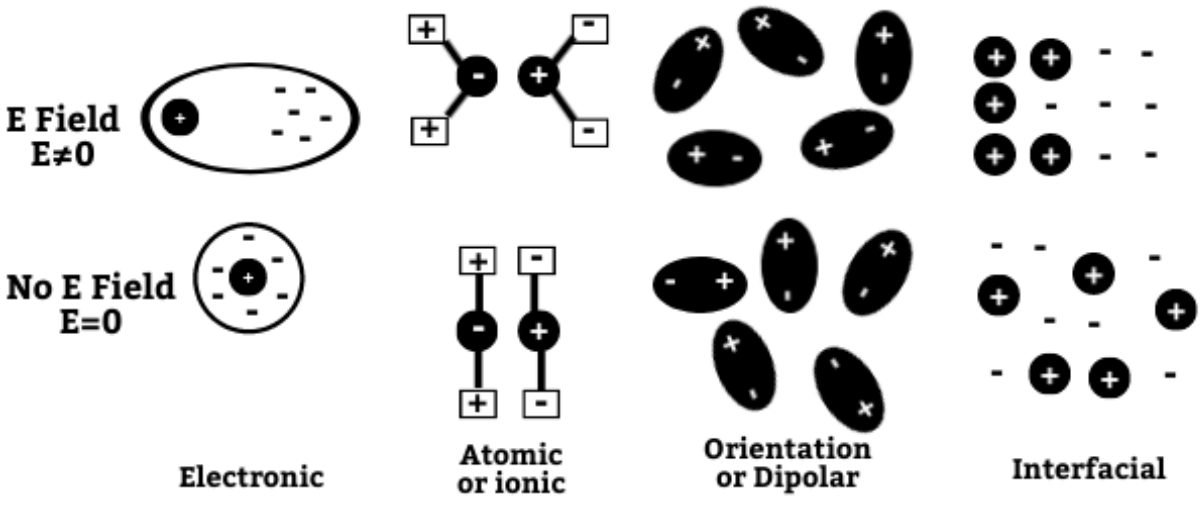

Figure 2. 7. Different polarization mechanisms. Adapted with permissions from [35]. Copyright 2011 John Wiley and Sons.

2.3.2 Microwave Properties

The microwave field undergoes continuous fluctuations in both direction and magnitude over time, consequently leading to a corresponding variability in the polarization of materials. This polarization response arises from the concerted efforts of ions or dipoles within the material to realign themselves with the frequency of the incident electromagnetic wave [31]. However, this reorientation process experiences a delay known as the relaxation time, which represents the time required for dipole rotation to occur. When the frequency of the microwave is raised, the rotational capability of dipoles fails to match the rapid alterations in the electric field, further exacerbating the disparity between the two phenomena. As a result, the polarization suffers from a lag phase in relation to the electric field [29]. This intricate interplay between the dynamic microwave field,

the material's polarization, and the concept of relaxation time serves as a fundamental aspect of electromagnetic interactions.

It is crucial to have a comprehensive understanding of parameters dictating the dielectric properties of a material. These parameters are crucial for microwave heating [31]. During the process of heating dielectric materials, it is commonly assumed that the magnetic field's contribution to microwave absorption is negligible. Instead, microwave absorption and subsequent heating predominantly occur due to the electric field's effects on the dielectric properties of the material [33].

Permittivity is a fundamental property that exerts a significant influence on microwave interaction, governing the dielectric response of materials [38]. Therefore, permittivity is described in terms of relative complex permittivity, denoting the ratio of a material's complex permittivity to the permittivity of free space [38]:

$$\varepsilon^* r(\omega) = \varepsilon' r(\omega) - j\varepsilon'' r(\omega) = \frac{\varepsilon^*(\omega)}{\varepsilon_o} = \varepsilon'(\omega) - j\varepsilon''(\omega) \quad \textbf{(2.6)}$$

where ω is radial frequency, $\varepsilon^*_r(\omega)$ is relative complex permittivity, $\varepsilon^*(\omega)$ is complex permittivity, ε_0 is the permittivity of free space with a constant value of 8.854×10^{-12} F/m, $\varepsilon'_r(\omega)$ is relative real permittivity, $\varepsilon'(\omega)$ is real permittivity, $\varepsilon''_r(\omega)$ is relative imaginary permittivity, $\varepsilon''(\omega)$ is imaginary permittivity and $j = \sqrt{-1}$.

The real permittivity, also known as the dielectric constant, measures the ability of a material to store electrical energy from the applied electromagnetic field, where as the imaginary permittivity, referred to as the dielectric loss factor, measures the ability of a material to dissipate microwave energy in the form of heat [30]. A high loss factor indicates that the material will absorb microwave

and heat readily, while a low loss factor means the material is microwave transparent, exhibiting minimal absorption [38].

Once the permittivities are calculated, then the loss tangent (tan δ) can be derived, representing the ability of a material to absorb microwave radiation [31]. Loss tangent conveys the relationship between real and imaginary permittivity. This term refers to the angle (loss angle) the material deviates from the electric field. The combined real and imaginary components constitute the complex permittivity, with the loss angle defined as being between the electric field and the complex permittivity. This loss tangent can be used to quantify the proportion of stored energy that dissipates during each cycle of field oscillation [39]. The loss tangent is given by the ratio of imaginary permittivity to real permittivity:

$$tan\delta = \frac{\varepsilon''(\omega)}{\varepsilon'(\omega)} \quad \textbf{(2.7)}$$

Optimum microwave energy coupling is observed in materials with high imaginary permittivity and moderate real permittivity [32], and hence they heat best in response to microwave [30].

Another parameter that can be determined from permittivities is the penetration depth (D_p), defined as the distance from the surface of the material at which the power reduces to 1/e from its actual value at the surface [37], or in other words half-power penetration depth which is the depth at which the incident power is dropped by one half [30]. Penetration depth holds significant importance when it comes to designing and scaling up a microwave heating system [40], and is given by the following equation:

$$D_p = \left(\frac{\lambda_o}{2\pi(2\varepsilon')^{1/2}}\right)\{[1 + (tan\delta)^2]^{1/2} - 1\}^{-1/2} \quad \textbf{(2.8)}$$

where λ_o is the incident wavelength. The penetration depth increases with increasing wavelength and decreases with increasing frequency and loss tangent. At low frequencies, penetration depth is higher but the actual amount of heat developed may not be substantial enough provided the intensity of the internal field is less [30]. Bulk heating is seen when the material size is close to the penetration depth [38]. When penetration depth is smaller than the material size, uniform heating is not observed as most of the heating occurs only at the surface and internal heating takes place via conduction [36]. Materials which are highly conductive, like metals with high real and imaginary permittivities values, are technically lossy or high loss material and have low penetration depth, thus the microwaves are reflected [30], [38]. In contrast, materials with low loss factors are microwave transparent and exhibit a higher penetration depth [38].Such materials almost completely transmit microwaves with minimal energy loss [41]. For effective microwave heating of the processing substance, the penetration depth should be comparable to the sample dimensions [41].

The dielectric properties of materials exhibit variability concerning temperature and frequency, as well as in response to factors such as purity, chemical state, and the specific manufacturing process employed [33]. Microwave properties such as penetration depth, permittivities and loss tangent determine if the material is a microwave absorber. Thus, these characteristics should be closely examined before selecting materials for such purposes [31].

2.4 Microwave heating involving carbon

Carbon materials are good microwave absorbers. They heat up when irradiated by microwaves, and can be used to heat other materials indirectly, or act as a catalyst and microwave receptors [32]. The dielectric loss tangents of various carbons are provided in Table 2.2. Notably, the loss tangents of the majority of carbon materials, with the exception of coal, exceed the loss tangent of

distilled water (0.118 at 2.45 GHz and 298 K). This highlights the significantly higher capability of carbon materials to absorb and convert microwave energy into heat compared to distilled water [32], [42]. However, in carbon materials like graphite, the reflective nature of the highly-ordered π–π conjugated structure restricts the efficient absorption of microwave energy and affects the overall heating performance of these materials [36].

Table 2. 1: Dielectric loss tangents for different carbon materials at frequency of 2.45 GHz and room temperature. Reproduced with permission from [32]. Copyright 2010 Elsevier.

Carbon material	**tanδ**	**References**
Coal	0.02-0.08	[39], [43]
Carbon foam	0.05-0.20	[44]
Charcoal	0.11-0.29	[45], [46]
Carbon black	0.35-0.83	[47], [48]
Activated carbon	0.57-0.80	[46], [49], [50]
Activated carbon*	0.22-2.95	[51]
Carbon nanotube	0.25-1.14	[52], [53]
CSi nanofibres	0.58-1.00	[54]

*Activated carbon at a mean temperature of 398 K.

2.5 Microwave heating mechanism in carbon

Electron-rich solids, like carbon materials with π-electrons, have been extensively studied in the context of microwave heating [55]. A prevailing hypothesis in the field suggests that interfacial polarization (Maxwell-Wagner-Sillars polarization) serves as the primary mechanism during microwave heating of solid carbon [55]. In carbon materials, the close conduction and valence bands facilitate the free movement of π-electrons, and the electric field component of microwaves can accelerate their motion [36], [56], [57]. Microwave-induced currents align in phase with the electromagnetic field, but since electrons cannot synchronize with the changing phase of the electric field, energy is dissipated in the form of heat in Maxwell-Wagner polarization [32], [58], [59].

However, a comprehensive assessment of the dielectric loss factor conducted across a broader range of parameters have shown that this type of polarization is indeed insufficient to fully explain the microwave heating mechanism in solid carbons [55]. While microwave heating of solutions primarily relies on the dipole rotation of polar solvent molecules, carbon materials which lack freely rotating dipoles, employ electron motion as the predominant heat-generating mechanism. This occurs through Joule heating in the grain or arc generation at phase boundaries [29]. This model of Joule heating is based on the classical theory that localized heat is produced due to the collision of free electrons with carbon atoms. This model finds significant support from numerous experiments and serves as an additional explanation for the heating mechanism involving carbon [36]. Moreover, carbon materials exhibit semiconducting characteristics attributed to the presence of delocalized π-electrons in the graphitic region, further contributing to Joule heating during microwave interactions [29].

Notably, microwave heating proves highly efficient and selective as microwave energy is predominantly absorbed by carbon material which is not the case in heating of solutions [29]. During microwave interaction, other intriguing phenomena can also take place, including an increase in electron kinetic energy, resulting in sparking and ionization in the surrounding medium, leading to plasma formation [29], [31], [32]. The different interactions which a solid carbon undergoes with a microwave radiation is depicted in Figure 2.8.

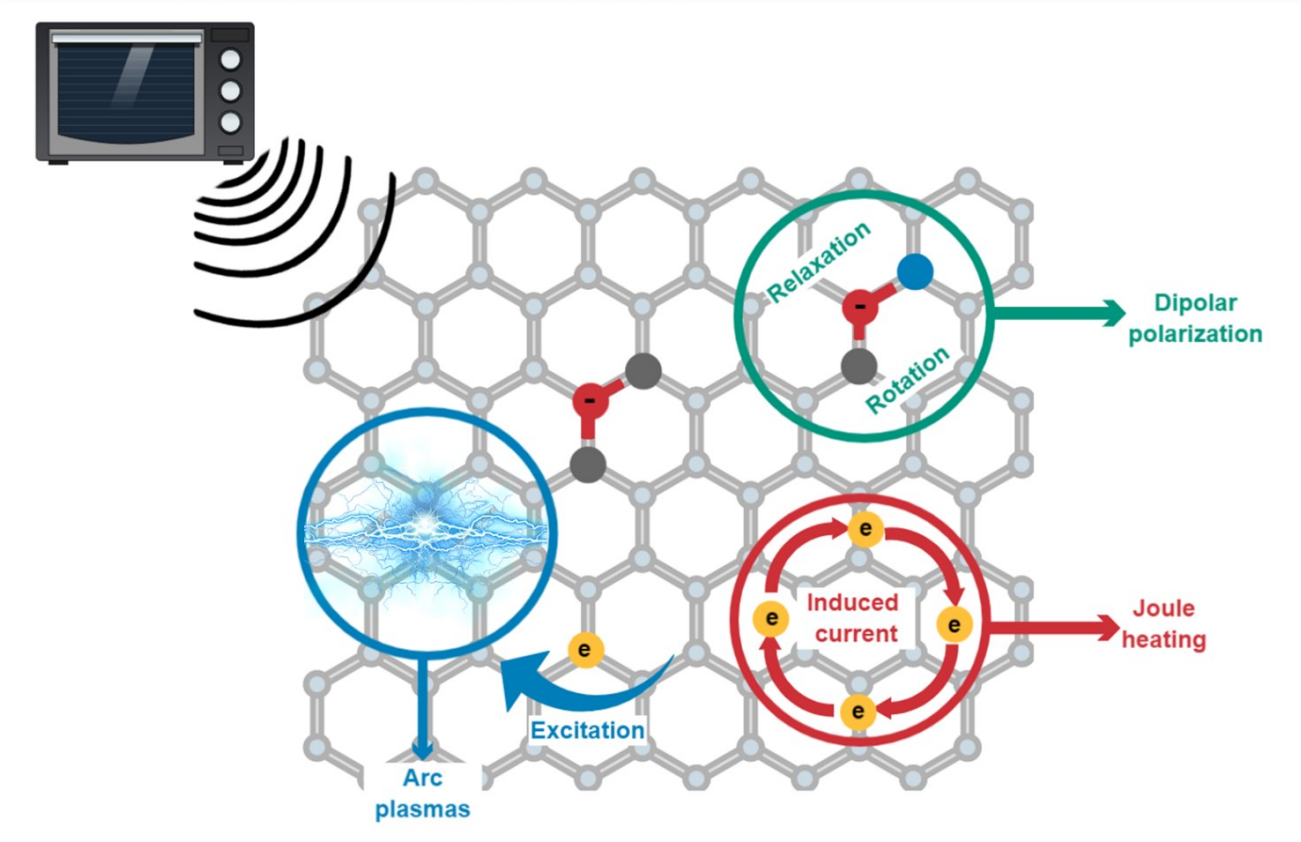

Figure 2. 8. Illustration of prevalent interaction mechanisms between a modern carbon and microwave field. Adapted with permission from [36]. Copyright 2021 Elsevier.

2.6 Carbon as a microwave receptor

Carbon materials exhibit a wide range of microwave absorption characteristics due to their outstanding thermal, mechanical, and electrical properties. Their diverse microwave absorption

capability allows them to actively participate in reactions, serving as heating media, hotspots or arc plasma generators [36]. The widespread usability of carbon materials is attributed to their affordability, ready availability in various textures, sizes, and forms [32]. In this manner, they can serve as intermediaries for heating materials that do not readily absorb microwaves (or are essentially microwave transparent), thus acting as microwave receptors to achieve indirect heating [32]. Carbon materials, thus, contribute to the reduction of time and energy consumption in synthetic processes [31], [60], [61].

Carbon as microwave receptors have been employed in processes such as biomass, oil shale, coal, glycerol and various organic waste pyrolysis [31], [32], [62], [63], [64]. Typically, these materials are not efficient microwave absorbers, making it challenging to directly heat them to the high temperatures required for complete pyrolysis [32].

Carbon materials have also been effectively used in soil remediation processes to remove organic pollutants [32]. The successful application of graphite fibers as microwave receptors in microwave-assisted extraction has been demonstrated for extracting contaminants from soils, rivers, and marine sediments [65]. Similarly, microwave-induced thermal treatments utilizing granular activated carbon as a microwave absorber have been utilized to reach suitable temperature for soil decontamination [32], [66].

Chapter 3
Investigating the microwave properties of carbon materials from microwave-driven methane pyrolysis[1]

3.1 Introduction

In recent years, the global community has witnessed a significant and concerning surge in CO_2 emissions, leading to the intensification of the greenhouse effect and posing a grave threat to the Earth's climate system. Scientific studies have determined that CO_2 alone accounts for approximately 20% of thermal absorption, making it a significant driver of the observed warming patterns [6]. The combustion of fossil fuels emerges as the primary source of anthropogenic CO_2 emissions, standing as the largest contributor to the overall greenhouse gas supply [7].

The continuous growth of the global population has resulted in an increasing demand for energy, which further exacerbates CO_2 emissions and adds to the environmental challenges we face [1]. This rise in energy consumption is driven by various factors, including industrialization, urbanization, and improvements in living standards across the world. As a consequence, there is a pressing need to explore and implement alternative energy solutions that can effectively mitigate CO_2 emissions and reduce the environmental impact associated with traditional fossil fuel usage. Despite the growing awareness of the need to transit to cleaner energy sources, fossil fuels are projected to remain the primary energy source for the next two decades. This projection is primarily attributed to their widespread availability and existing infrastructure, which makes the shift to alternative energy sources a complex and challenging task [1]. However, it is imperative

[1]A version of this chapter has been published in Carbon Trends Journal and appears as: Manzoor, S., Wani, O. B., & Bobicki, E. R. (2024). Investigating the microwave properties of carbon materials from microwave-driven methane pyrolysis. Carbon Trends, 100326.

that we address the urgent need for the development and implementation of CO_2 -neutral energy alternatives.

In this pursuit, hydrogen has emerged as a highly promising alternative. Its viability is rooted in a range of desirable characteristics, including high efficiency, versatility, an inexhaustible supply, convenience, and independence from foreign control [3]. By harnessing hydrogen as a clean fuel source, substantial reductions in CO_2 emissions and other harmful pollutants resulting from the combustion of fossil fuels can be achieved [9]. However, the current benchmark process for hydrogen production, known as steam reforming of methane followed by the water-gas shift reaction, presents a significant challenge due to the substantial CO_2 by-product generated in the process [10]. Although the produced hydrogen can be utilized as a clean fuel, the associated CO_2 emissions pose environmental concerns. As a result, alternative hydrogen production processes have garnered significant interest. These processes aim to address the limitations of the steam reforming method by either reducing CO_2 emissions or improving hydrogen yields. However, alternative hydrogen production processes face their own set of challenges. Some processes that aim to minimize CO_2 emissions tend to be cost-prohibitive due to the additional infrastructure required for capturing and storing the CO_2 [1]. Catalytic pyrolysis of methane is yet another method, however, it has a major disadvantage as the catalyst used is deactivated by carbon surface deposits, which need to be burned to restore the original catalytic activity, thus generating CO_2 as a by-product [19]. Other methods, such as biomass gasification or electrolysis, while offering potential for CO_2 reduction, often have lower hydrogen yields and are still in the early stages of development, making them less economically viable at present [12].

Recently, microwave pyrolysis of methane has emerged as an innovative approach for achieving dual objectives: the production of clean hydrogen fuel and the capture of carbon that would

otherwise be emitted as CO_2 during combustion [14], [15], [67]. This method involves subjecting natural gas to microwave radiation while utilizing microwave carriers (like carbon) to facilitate heat transfer to the gas. As a result, gaseous hydrogen and solid carbon are produced [15]. It is noteworthy that the solid carbon component accounts for up to 75% of the resulting product's mass in methane pyrolysis, highlighting the need for a comprehensive analysis to gain deeper insights into the process [14]. One notable advantage of carbon materials in this context is their excellent microwave absorbing properties. This characteristic enables their participation in reactions as heating media or indirectly heating microwave-transparent materials [32]. To further advance the development and widespread implementation of microwave pyrolysis technology, it is crucial to accurately measure the microwave properties of carbon. These properties encompass real and imaginary permittivity, loss tangent, and half-power penetration depth. The aforementioned properties not only contribute to establishing heating characteristics of material but are also observed to be influenced by factors like frequency, temperature, material type, and so on. Real permittivity or dielectric constant (ε') governs the efficiency of energy storage in materials when exposed to an electric field, while imaginary permittivity or dielectric loss factor (ε") determines the extent to which a material dissipates stored energy as heat [30].

The following equation gives the relative complex permittivity, $\varepsilon^* r(\omega)$ with $j = \sqrt{-1}$.

$$\varepsilon^* r(\omega) = \varepsilon'(\omega) - j\varepsilon''(\omega) \quad \textbf{(3.1)}$$

The loss tangent and half-power penetration depth are defined in Equations 3.2 and 3.3 [31], [37].

$$tan\delta = \frac{\varepsilon''(\omega)}{\varepsilon'(\omega)} \quad \textbf{(3.2)}$$

$$D_p = \left(\frac{\lambda_o}{2\pi(2\varepsilon')^{1/2}}\right)\{[1 + (tan\delta)^2]^{1/2} - 1\}^{-1/2} \quad \textbf{(3.3)}$$

Where ω is the angular frequency and λ_o is the microwave wavelength in free space.

Understanding the complex permittivity of materials is of utmost importance in comprehending their behaviour within a microwave field and regulating heating characteristics. This knowledge plays a vital role in scaling up processes and designing efficient industrial systems [38]. It is essential to have information about the permittivities as a function of both temperature and frequency. While a particular microwave application might use a single frequency, understanding the frequency dependency is crucial for characterizing the relaxation processes in the material. Moreover, having knowledge of the permittivities can aid in selecting the most suitable operating frequency for the treatment process or industrial application [30], [38]. Additionally, it can also provide valuable insights into material conductivity, polarity, relaxation processes, and resonant behaviour, enabling a deeper understanding of their properties [38].

The present work investigates the microwave properties of carbon (seed carbon; SC and product carbon; PC) from room temperature to 1250°C as well as thermogravimetric analysis (TGA), differential scanning calorimetry (DSC) and X-ray diffraction (XRD) of the samples to better explain the permittivity results.

3.2 Methods and Materials

3.2.1 Materials

The materials utilized in this study consisted of two carbon samples, out of which one is a commercially available activated carbon sample and the other is obtained from microwave-driven methane pyrolysis experiments conducted at the University of Toronto [68]. The first sample, referred to as seed carbon (SC), served as the precursor activated carbon derived from bituminous coal. The second sample, known as product carbon (PC), comprised the carbon particles produced

as the end product of the pyrolysis process. To facilitate testing, both samples were used in the form of loose powder with particle sizes ranging from 250 to 600 μm. In addition to the carbon samples, graphite flakes in the same particle range were also included in the thermal analysis for comparative purposes. SC was assessed for moisture content (4.6 wt.%), volatile matter (3.6 wt.%), ash (1.5 wt.%) and fixed carbon (90.3 wt.%) using a TA Instruments Discovery thermogravimetric analyzer, and for total sulfur (0.154 wt. %) using strong mineral acid block digestion followed by ICP-OES (inductively coupled plasma-optical emission spectroscopy). PC was not assessed for this as it is produced from natural gas and will be completely free of moisture and ash. When exposed to temperatures of 1250°C, it will undergo complete conversion into fixed carbon (98.50%) [14] with no remaining volatile matter.

3.2.2 Thermal Analysis

Thermal properties of ground seed carbon (SC), product carbon (PC), and graphite samples, such as thermogravimetric analysis (TGA) and differential scanning calorimetry (DSC) was performed using a Netzsch STA 409 PC/PG instrument at Brockhouse Institute for Materials Research (BIMR) Thermal Lab, Hamilton, ON, Canada. The samples of 126-147 g mass were carefully placed in alundum crucibles and subjected to a controlled heating process from room temperature up to 1250°C at a heating rate of 10°C/min. To maintain a neutral environment during the analysis, argon gas was employed at a flow rate of 20 mL/min. This experimental setup facilitated the simultaneous monitoring of both heat flow and mass loss of the samples as the temperature increased.

3.2.3 Permittivity measurements

The real and imaginary permittivities of the samples were determined using the cavity perturbation technique at Microwave Properties North (MPN), Deep River, ON, Canada [69], [70]. This

technique is based on quantitatively assessing the effect of sample, along with sample holder, on a precisely defined electric field within a cavity across various frequencies and temperatures [38]. Figure 3.1 shows the diagram for cavity perturbation technique. The effect of empty sample holder is assessed under identical conditions and subtracted from the overall measurements. These changes are recorded as a function of temperature, frequency, and elapsed time. By analyzing the obtained data, the two-component complex dielectric constant was determined, specifically the real and imaginary permittivities (ε' and ε''), in relation to frequency and temperature.

The permittivity measurements were conducted under a flow of 5 standard cubic centimeters per minute of ultra-high purity argon gas, spanning from room temperature to 1250°C in increments of 50°C at frequencies of 397, 912, 1429, 1948 and 2467 MHz. This temperature was chosen as methane was observed to reach a 90% conversion at 1216°C [15]. Measurements were also recorded as the temperature was reduced in increments of 50°C, returning to 100°C and then to room temperature. To replicate the conditions of carbon used in methane pyrolysis experiments, loose powder form with particle sizes ranging from 250 to 600 μm was utilized instead of pressed pellets in the cavity perturbation technique. A "flow-through" holder was employed, incorporating a porous quartz frit inserted against the base (Figure 3.2a). The argon gas was directed to flow through the frit and the powder sample. Initially, the gas flow bypassed the frit edges, resulting in significant activity and bouncing of the powder with low flows of approximately 10 standard cubic centimeters per minute of argon. To address this issue, a plug was positioned at the top of the holder, ensuring a secure mechanical fit (Figure 3.2b). This adjustment successfully altered the flow patterns, achieving a stable state for the powder, free from disturbances.

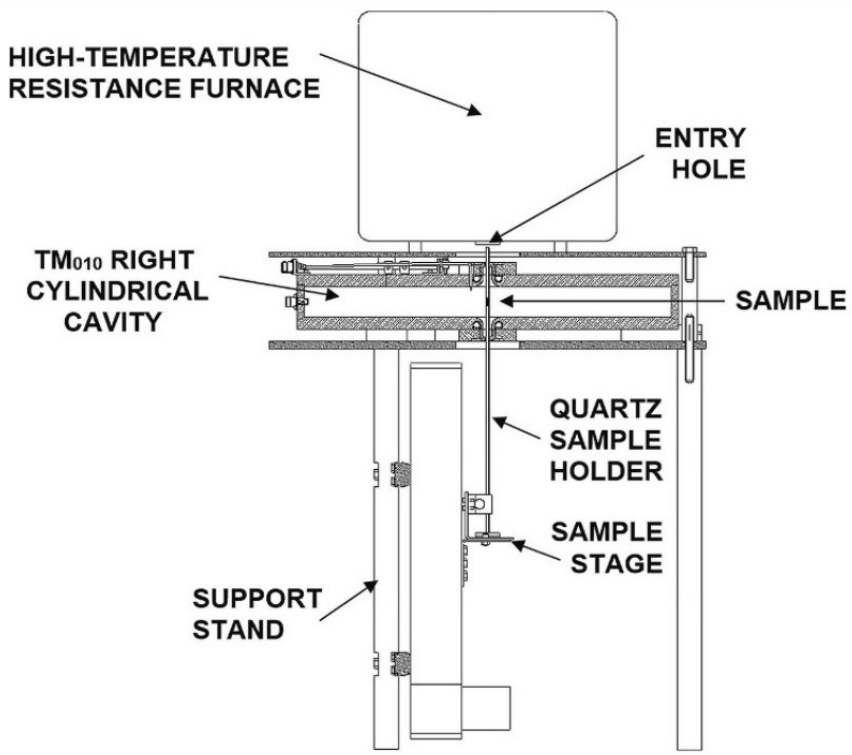

Figure 3. 1. Schematic diagram of the cavity perturbation apparatus at Microwave Properties North. Reproduced with permission from [71]. Copyright 2023 Elsevier.

Figure 3. 2. a) Initial SC on frit in holder b) SC in holder with plug.

3.2.4 X-ray Diffraction Analysis

The X-ray diffraction (XRD) patterns of SC, PC and graphite flakes were acquired using a Bruker D8 Advance diffractometer. Cu-Kα radiation with a wavelength (λ) of 1.5418 Å was employed for the measurements, covering a 2θ range from 5° to 110°. Subsequently, Origin Lab software was utilized to perform background removal and multipeak fitting analyses on the obtained patterns. The resulting data included the full width at half maximum (FWHM) values and peak positions.

To further characterize the materials, the FWHM values and peak positions were employed in the Scherrer equation [72], [73] to calculate the lateral size (La) and stacking height (Lc) of the samples:

$$L_a = \frac{1.84\lambda}{\beta_a \cos(\theta_a)} \quad \textbf{(3.4)}$$

$$L_c = \frac{0.89\lambda}{\beta_c \cos(\theta_c)} \quad \textbf{(3.5)}$$

In the above equations, βa and βc correspond to the FWHM of the fitted 101 peak and 002 peak, respectively, and θa and θc indicate the Bragg angles of the corresponding peaks.

3.3 Results and Discussion

3.3.1 TGA/DSC Analysis

SC, PC and graphite were tested using thermal analysis (TGA and DSC). Figure 3.3 illustrates the change in mass and heat flow with increasing temperature from 25°C to 1250°C. SC underwent an initial 5% mass loss with a matching endothermic peak (100-155°C) which is associated with the loss of loosely bonded free water and volatile compounds [14]. Raw activated carbon particles typically exhibit absorption of water vapour on their extensive surface area [14], [74], [75] which is removed when subjected to heat at temperatures below 150°C [14]. The effective adsorption capability of activated carbon is typically associated with its elevated specific surface area, porosity, and pore volume [76]. Cuhadaroglu et al., found similar results with bituminous coal-derived activated carbon that underwent a 7% mass loss up to 150°C [77]. The continued gradual mass loss at higher temperatures is due to other volatile materials being released from the sample. As illustrated in Table 1, it is evident that SC comprises 3.6% of volatile matter and 0.154% of sulphur. These constituents undergo evaporation at elevated temperatures, resulting in a corresponding reduction in mass [78]. As expected, this behaviour was not observed in either graphite or PC samples as they are formed at methane cracking temperatures of above 1000 °C.

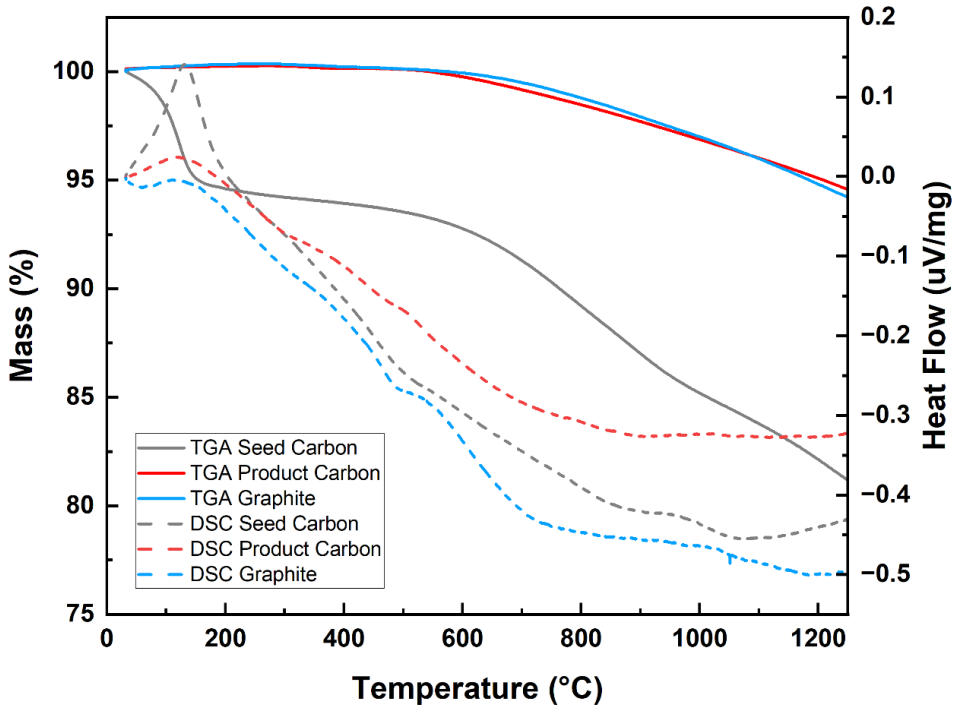

Figure 3. 3. TGA and heat flow versus increasing temperature for SC, PC and graphite.

3.3.2 Microwave properties measurements

Figure 3.4 and 3.5 depict the real and imaginary permittivities of SC and PC at frequencies 397, 912, 1429, 1948 and 2467 MHz as a function of increasing temperature. Both permittivities for each sample exhibit similar trends and were frequency dependent. In the case of SC, the permittivities declined between room temperature to 200°C which correlates well with the mass loss and endothermic peak seen in Figure 3.3 over this temperature range. This reduction in permittivity is ascribed to the release of free water adsorbed by SC from atmosphere as also seen in other literature [74]. The decrease in permittivity is linked to the elimination of the impact of this polar species, alongside a decrease in the quantity of material available for interaction with the electric field [30], [78]. As the temperature further increased, the permittivity values remained

stable due to the water being completely eliminated [74]. Additionally, the removal of volatile matter does not impact the overall permittivities significantly as volatile hydrocarbons have low permittivity [78], [79]. The values demonstrated a rapid increase after the critical temperature was achieved which is mostly seen in microwave-responsive materials [30]. This observation is consistent with a previous study on microwave drying of coal [78]. The study indicated that graphitization becomes evident at temperatures exceeding 550°C, leading to a decline in electrical resistance as the temperature rises. As a result, the conductivity of the char starts to surge significantly with temperature, causing a rapid escalation in permittivity. This exponential increase is accountable for the occurrence known as thermal runaway [78]. It can be seen in Figure 3.4 that after the permittivities reached a peak, they started to decline at very high temperatures of 860-960°C. This phenomenon can be explained by the high conductivity observed at elevated temperatures, leading to non-uniform electric fields within the sample, reducing penetration depth and causing the material to exhibit reduced efficiency in absorbing microwaves [30].

Generally, at low temperatures, the frequency dependency of permittivity is very low and this is due to electrons or ions being displaced slightly but rapidly. As the temperature increases, their displacement increases and the permittivity as well as its dependency on frequency also increases [30].

Although undulations are seen in the plots of PC, the permittivity remains reasonably consistent for 912 MHz and 2467 MHz frequencies which is close to the industrial (915 MHz) and domestic (2450 MHz) frequencies. Consistent values mean there is low probability of thermal runaway and PC will be easy to operate in microwaves.

Overall, the permittivity values are high which implies that both samples have good absorbing ability and are excellent microwave susceptors. Materials with a high carbon content tend to

display greater dielectric constant values, primarily due to the substantial polarization developed by the presence of delocalized π-electrons. These electrons move freely, leading to ionization within the surrounding atmosphere [80], [81]. The magnitude of real permittivity values in SC is larger than that seen in PC. This means that SC is more effectively polarized by the microwave fields over the temperature range. Similarly, imaginary permittivity values were also greater in SC when compared to PC.

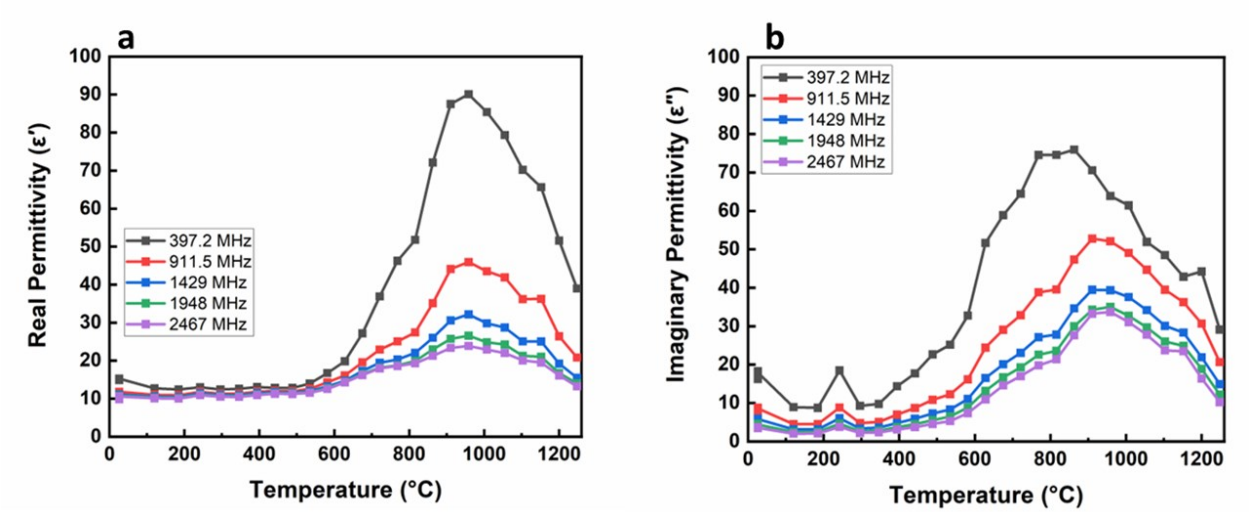

Figure 3. 4. Real (a) and imaginary permittivities (b) vs temperature of SC.

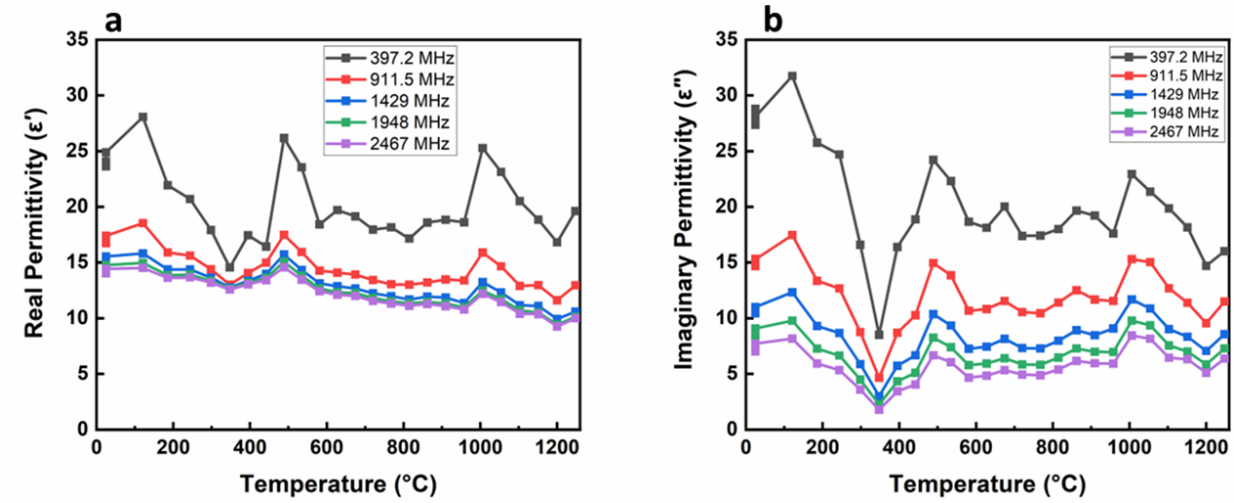

Figure 3. 5. Real (a) and imaginary (b) permittivity vs temperature of PC.

The real permittivity for both samples upon heating and cooling at 2467 MHz is shown in Figure 3.6. In the case of SC, the variation that was detected during the heating phase was not observed during the cooling phase. Rather, it maintained a relatively stable value throughout the cooling cycle. This implies that whatever factor contributed to the changes in real permittivity upon heating was either eliminated or irreversibly modified due to the temperature rise. In the plot for PC, the reversible peak is evident upon cooling and remained largely unchanged.

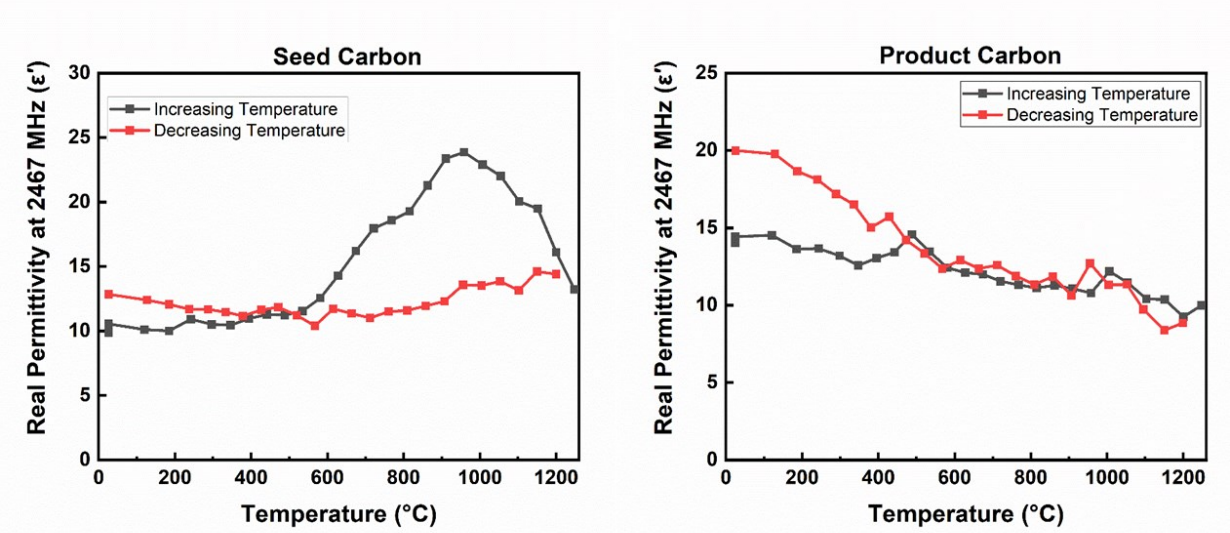

Figure 3. 6. Real permittivities for SC (a) and PC (b) during heating and cooling cycle.

Figure 3.7 shows loss tangent (or dissipation factor) of SC and PC which is the ratio of imaginary permittivity to the real permittivity. It is evident that the loss tangent exhibited a resemblance to the behaviour of the imaginary permittivity. Loss tangent indicates the ability of a material to absorb microwaves effectively and exhibit efficient heating when exposed to it [30]. The figure shows high values for the loss tangent, meaning that both the samples will absorb microwaves and heat readily. SC, however, represents a material in which the imaginary permittivity and, consequently, the loss tangent exhibit a sharp increase as the temperature rises beyond a critical point. As a consequence, SC becomes more adept at absorbing microwave energy, leading to a rapid temperature rise in the material. As the loss tangent also surges even further, energy absorption can escalate exponentially and, in turn, trigger thermal runaway [82]. This phenomenon is also explained in previous sections. Thermal runaway leads to unfavourable hot spots in material, but it can also be deliberately harnessed to achieve rapid and efficient heating of materials [82], [83]. However, in case of the microwave-driven pyrolysis process, thermal runaway is not desirable. Carbon may overheat and in the presence of air may combust.

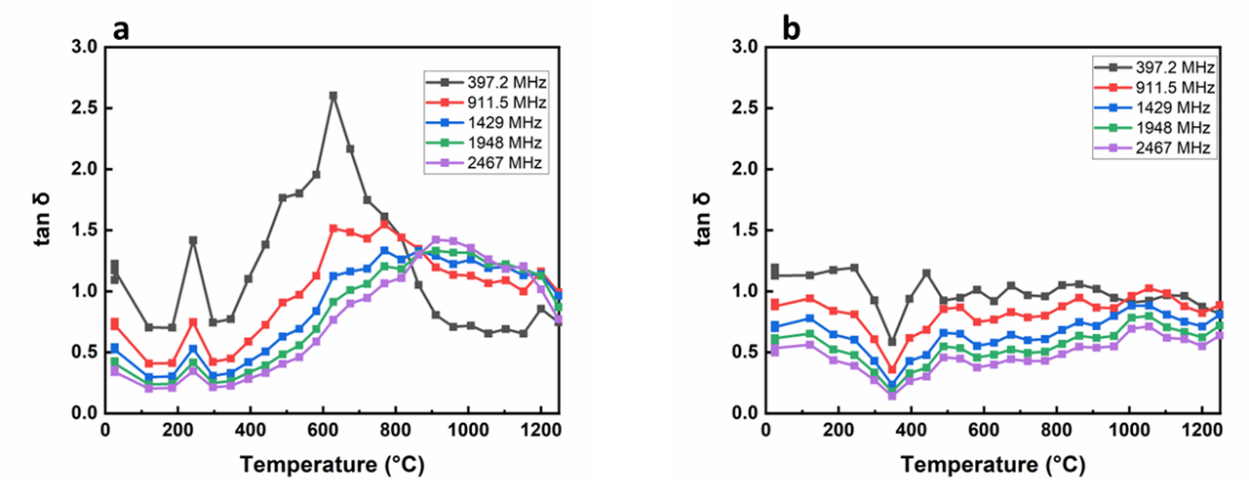

Figure 3. 7. Loss tangent vs temperature for SC (a) and PC (b).

The half-power depth for SC and PC is shown in Figure 3.8. It is the depth at which the power is reduced by one-half and is inversely proportional to permittivities. This plot is consistent with the permittivity plots. Effective heating of a substance can be achieved using microwaves when the half-power depths are comparable to the dimensions of the sample [41]. The plot shows that the half-power depth decreases with an increase in frequency. In our case, SC and PC exhibited half-power depth in the range of 1-10 mm which is favourable to the methane pyrolysis system. This aligns with the general observation that materials with high efficiency in converting microwave energy to heat tend to exhibit shallow penetration depths at a fixed frequency [41]. Additionally, this indicates that the microwaves can penetrate and heat the material evenly throughout its volume, resulting in efficient heating. SC and PC can be used as microwave carriers during the methane pyrolysis process, thus making the process self sufficient and eliminating the need for expensive catalysts.

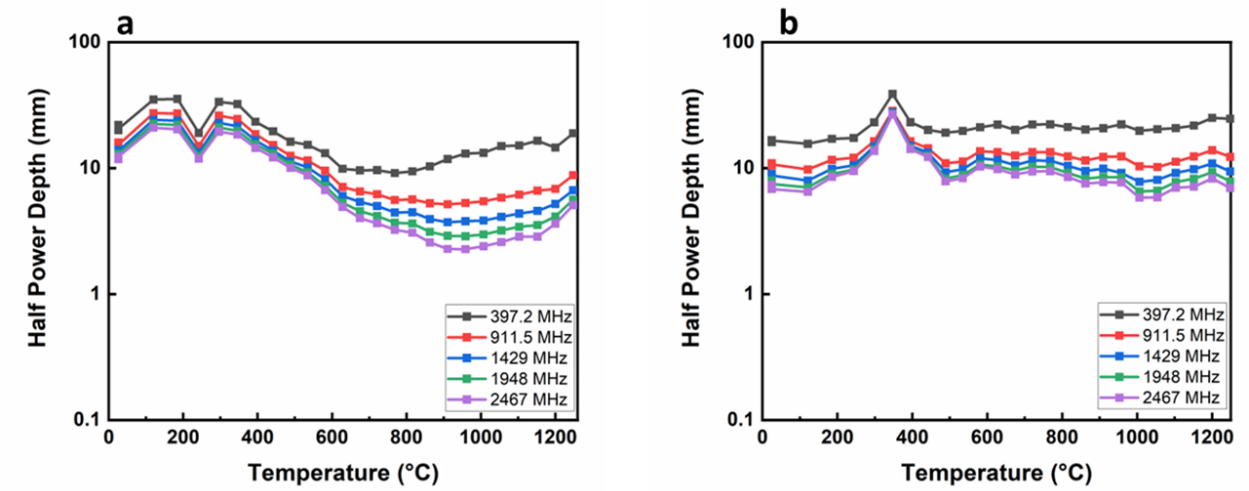

Figure 3. 8. Half-power depth for SC (a) and PC (b) vs temperature.

3.3.3 XRD

The XRD analysis (Figure 3.9) for the samples reveal that the peaks observed at 2θ = 24.8° to 26.4° correspond to the 002 reflection, while the peaks at 2θ = 43° to 43.7° correspond to the 101 reflection. The second peak observed in the XRD pattern of graphite at 2θ = 54.5° is attributed to the 004 reflection. The broad diffraction peaks observed in the XRD patterns of SC and PC indicate an amorphous carbon structure. In contrast, the peaks of graphite are sharp, indicating a crystalline form.

The SC used in this experiment is activated carbon derived from bituminous coal. Activated carbon typically exhibits an amorphous structure with random microcrystalline carbon fragments [84]. The presence of the two broad diffraction peaks at 2θ = 24.8° and 43.7° indicates a disordered amorphous nature.

The PC, on the other hand, has undergone heating at ~1220°C during microwave pyrolysis. As a result, there is a shift in its 002 peak at 2θ = 25.1° to the right when compared to 002 peak at 2θ = 24.8° for SC. This shift, along with the narrowing of the peak width, suggests that the PC has

undergone graphitization [14]. Previous studies have reported the graphitization of amorphous carbon to crystalline graphite under microwave heating in the presence of a catalyst [55]. While complete graphitization did not occur in this case, as it requires high temperatures of 3000°C, some degree of ordered structure was achieved in the PC, as indicated by the shifted and sharpened 002 reflection peak. L_c and L_a values for all samples are given in Table 3.1. The increase in these values for PC from SC suggest that the potential existence of a crystalline structure [14]. A comprehensive characterization of both SC and PC has been provided in our previous published work [14], [67].

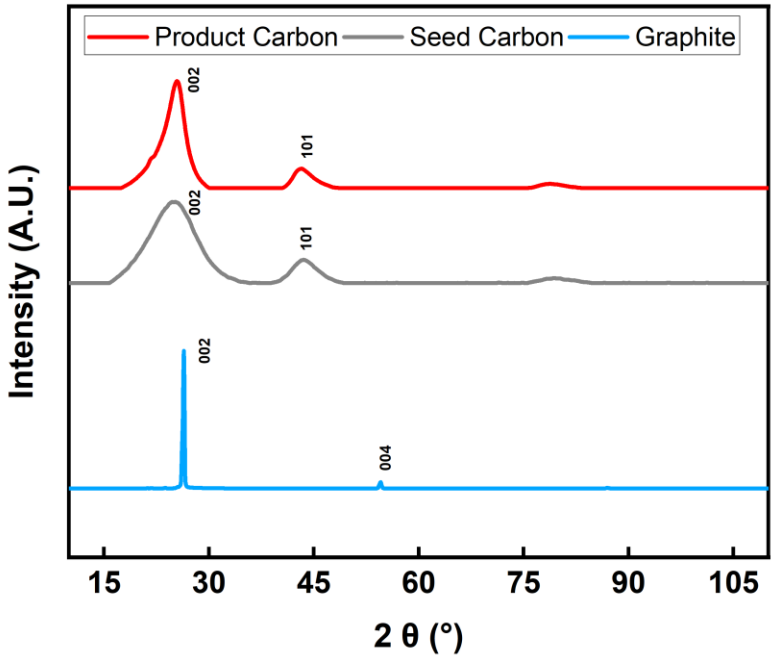

Figure 3. 9. XRD pattern for SC, PC and graphite.

Table 3. 1. Lateral size (L_a) and stacking height (L_c) for SC, PC, and graphite flakes.

Sample	**L_c (nm)**	**L_a (nm)**
SC	1.0	4.0
PC	2.2	5.3
Graphite	26.1	-

3.4 Scalability and Applications of Methane Microwave Pyrolysis

The drive towards decarbonization is gaining substantial traction across diverse industry sectors as they embrace cleaner energy sources. Hydrogen, recognized as a promising solution for energy supply and emissions reduction, must adhere to environmentally friendly production methods to genuinely contribute to decarbonization. This involves capturing and storing carbon dioxide emissions during production and utilizing electricity from clean sources. Currently, water electrolysis stands out as a prevalent and environmentally friendly hydrogen production method. However, industrial practices often involve using precious metals like iridium for electrodes, rendering the process technically feasible but economically impractical [85], [86]. In contrast, microwave methane pyrolysis, though in its early stages, presents a promising alternative. This method generates solid carbon as a byproduct (approximately 3 kg-C/kg-H2 [15]), effectively eliminating CO_2 emissions from the loop. The resulting solid carbon can be used again in the microwave pyrolysis process [15], and can therefore serve as a cost-effective heat carrier for methane gas, making the process economically viable compared to water electrolysis. In addition to the major product hydrogen gas, the secondary product- solid carbon can be used in applications such as automobile tires, battery electrodes, construction materials, carbon columns, reduction of iron oxide etc. thereby generating additional revenue. Furthermore, results from this study have indicated that the solid carbon generated as a byproduct has the ability to be a microwave carrier- this means that the only cost associated would be for the initial activated carbon to start the reaction. As the reaction progresses, the product carbon would suffice as the heat carrier and thereby make the process sustainable in itself, eliminating the need for activated carbon or costly catalysts thereby making the process economically feasible. The major advantage of this process so far lies in removing the carbon dioxide from the hydrogen synthesis loop-i.e., negating any CCS technique as the byproduct is directly solid carbon. While still in small-scale testing, this

technology shows potential for economically efficient hydrogen production, contingent upon methane availability and a clean electricity source.

Microwave absorbers, critical in numerous applications for efficiently converting electromagnetic energy into heat, hinge on the dielectric loss tangent—a key parameter defining a material's microwave energy absorption and heat generation capabilities [32]. Microwave heating, with its distinct advantages over conventional methods, encompasses non-contact heating, rapid and selective material heating, volumetric heating, quick start-up and stopping, interior material body heating, and enhanced safety and automation [32], [87], [88], [89], [90].

Carbon materials, distinguished by a high dielectric loss factor, emerge as exemplary microwave absorbers, making them well-suited for diverse applications such as soil remediation, biomass pyrolysis, organic waste treatment, and catalytic heterogeneous reactions [32]. Various carbon materials like charcoal, carbon black, and activated carbon, exhibiting loss tangents ranging from 0.1 to 0.8, demonstrate microwave absorption capacities comparable to or surpassing distilled water (0.118 at 2.45 GHz and 298 K) [32]. This underscores their superiority in converting microwave energy into heat [32], [91], [92].

Our study's outcomes reveal elevated values of both real and imaginary permittivity, along with a high loss tangent, in both SC and PC, unequivocally validating the microwave-absorbing properties of the carbon materials used and affirming their potential as efficient microwave carriers. Importantly, the economic feasibility of utilizing carbon materials is highlighted by their cost-effectiveness compared to traditional metal catalysts like nickel, iron, and cobalt. This cost advantage, coupled with lower prices, enhanced fuel flexibility, absence of sulfur poisoning, lack of contamination in the carbon by-product, mitigation of CO_2 emissions, the elimination of the need for catalyst regeneration and the utility of carbon formed as a catalyst precursor, reinforces

the economic viability of incorporating carbon materials in methane pyrolysis [93], [94], [95], [96], [97], [98]. Furthermore, the intrinsic catalytic properties of carbon support its feasibility in methane pyrolysis, eliminating the need for external catalysts and separation processes, except during start-up operations [99], [100].

3.5 Conclusions

Microwave pyrolysis of methane has recently emerged as an innovative technique to tackle to problem of rising CO_2 emissions from hydrogen fuel production. To better understand and scale up this method, it was crucial to investigate the microwave properties of the carbon used and generated during the process. This study focused on examining the microwave characteristics of two carbon samples, namely seed carbon (SC), and product carbon (PC) obtained from the microwave-driven pyrolysis of methane. The cavity perturbation technique was employed across frequencies of 397, 912, 1429, 1948 and 2467 MHz, ranging from room temperature to 1250°C. The results revealed that SC initially exhibited a decrease in permittivity values up to 200°C, which can be attributed to moisture release from the sample. This observation aligns with the TGA/DSC results, which indicated a 5% mass loss at temperatures ranging from 100°C to 155°C. Subsequently, the permittivity gradually peaked and then started to decline due to high conductivity. In the case of the PC, the permittivity exhibited fluctuations but remained consistent. Since this form of carbon is generated at elevated temperatures, no moisture loss was observed in the TGA/DSC analysis. The results demonstrate that microwaves can evenly penetrate and heat both samples throughout their volume, resulting in effective and efficient heating. SC showed larger magnitudes of permittivity compared to PC, indicating its more efficient response to microwave fields. However, the possibility of thermal runaway in SC makes it less suitable for microwave-driven methane pyrolysis process. Moreover, XRD analysis indicated that both SC and

PC displayed structures of amorphous carbon, with PC exhibiting some signs of partial graphitization. Overall a good agreement was observed between TGA/DSC, XRD and permittivity tests. Results from this study suggest that the carbon produced during pyrolysis can facilitate as an effective microwave heating carrier avoiding the requirement of expensive catalysts.

The recommendations of this study include exploring the potential applications of carbon produced through microwave pyrolysis, particularly because of its semi-graphitic structure. Potential uses include steelmaking, graphene production, and as anode materials in Na-ion batteries, with a focus on thorough testing for these specific uses [101], [102]. While valuable insights have been gained from lab-scale tests, it is imperative to replicate experiments in realistic conditions to ensure accurate performance assessment. The use of activated carbon as the seed carbon in microwave-driven pyrolysis prompts the need to further explore alternative, more cost-effective, and environmentally friendly carbon sources, such as biomass, and to investigate their microwave properties. Additionally, a technoeconomic analysis comparing carbon generated by microwave pyrolysis to traditional carbon catalysts is essential for a comprehensive understanding of the industrial scale economic viability. Furthermore, conducting a life cycle assessment (LCA) of electricity used in microwave pyrolysis compared to electricity used in other hydrogen production methods will help in evaluating the environmental impact of this heating approach. By delving into these investigations, the efficiency of methane microwave pyrolysis and its applications can be enhanced, contributing to progress in developing a more sustainable and economical energy solution.

Chapter 4
Comminution of carbon particles in a fluidized bed reactor: A review[2]

4.1 Overview

Fluidized bed combustion is a popular method to convert fuel to energy owing to its fuel flexibility, low emissions, and efficiency [103], [104]. In this process, solid particles are characterized with fluid-like properties as they are evenly distributed and suspended in upward jets of air inside the combustor [105]. When fuel particles such as coal enter a combustion system, they are heated up quickly by bed materials at elevated temperatures, followed by decomposition. Internal high pressure is created as volatile gases are produced inside the coal particles. At the same time, impulsive forces result from the neighbouring particles while temperature gradient within the particles give rise to thermal stress. These factors play an important role in the comminution of coal particles [106].

Comminution phenomena, namely primary fragmentation, secondary fragmentation, percolative fragmentation and attrition occur either side by side with each other, or with combustion process [107]. Figure 4.1 presents the comminution phenomena in series/parallel. These phenomena create several challenges during combustion as they impact the reliability and efficiency of the process. The particle size distribution of fuel in bed is changed substantially which in turn affects the rate and mechanism of fuel conversion, and heat and mass transfer coefficients. Elutriation of fine particles from bed is another challenge due to comminution in fluidized bed combustion. This

[2] A version of this chapter has been published in Minerals Engineering Journal and appears as: Manzoor, S., Tatum, J., Wani, O. B., & Bobicki, E. R. (2023). Comminution of carbon particles in a fluidized bed reactor: A review. Minerals Engineering, 195, 108026.

occurs when particles get entrained in gas exit out of the reactor resulting in loss of unburnt carbon [108]. Fines arise from three sources; original feed, devolatilization process, and fragmentation during combustion [106]. Fines from original or monosized fuel feed are disregarded but those generated during attrition, fragmentation, and shrinkage of coarse particles to elutriables are considered a product of comminution [103], [106]. Such a loss of fines is detrimental to combustion efficiency and pollution control of fluidized bed reactor [106]. In this paper coal, char, biomass, waste derived fuels, and alternative fuels will be discussed as carbon-based fuels (Table 4.1) that experience comminution during fluidized bed combustion.

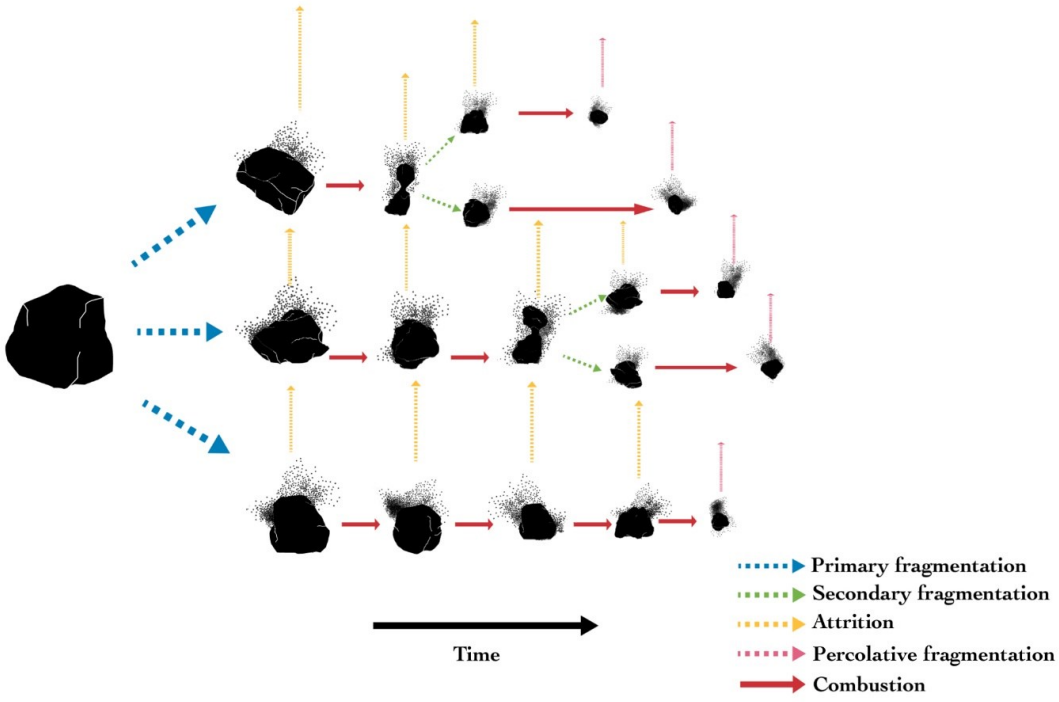

Figure 4. 1. Schematic diagram showing series-parallel comminution. Adapted with permission from [109]. Copyright 1991 Elsevier.

Table 4. 1. Different fuels used in fluidized bed reactor.

Feedstock	**References**
Coal and coal blends	[108], [110], [111], [112], [113], [114], [115], [116], [117], [118]
Alternative fuels (pre-dried sludges, civil wastes, and industrial wastes)	[119], [120], [121]
Biomass (wood, agricultural wastes, sawdust, rice husk, and ground seed corn)	[117], [119], [122], [123], [124], [125], [126], [127], [128]
Limestone	[129], [130], [131], [132]

4.2 Comminution Phenomenon

It is clear that comminution is an influential process occuring in fluidized bed reactor. A coal particle injected in a fluidized bed experiences subsequent events in the given order: heating and drying; devolatilization and volatile combustion; swelling and primary fragmentation; char combustion and secondary fragmentation; and attrition [133]. Table 4.2 summarizes the impact of different comminution phenomenon on bed of fuel particles. The different fragmentations which a fuel particle undergoes are presented in Table 4.2:

Table 4. 2. Impact of comminution type on the bed of fuel particles.

Comminution type	Cause	Product	References
Primary	Devolatilization, and thermal stress	Coarse particles, non-elutriable	[134], [135]
		Smaller fragments, elutriable	[135]
Secondary	Mechanical stress, and breakage of internal carbon bridges	Coarse particles, non-elutriable	[130], [133]
Percolative	Sudden collapse of internal connectivity	Fines, elutriable	[103], [136]
		Fines, non-elutriable	[134]
Attrition	Abrasion, chemical and thermal stress	Fines, elutriable	[130], [136]

4.2.1 Primary fragmentation

Primary fragmentation occurs immediately after a particle is introduced into a fluidized bed system [130], and undergoes a thermal shock as the particle heats up [107]. This phenomenon is considered to be the most crucial comminution process [137], as in case of coals or highly reactive fuels it greatly contributes to size reduction of particles [138], [139]. Primary fragmentation is always seen to be closely associated with devolatilization as there is build up of internal pressures in the porous network of the particle [134] by release of volatile gases or CO_2 emmisions [107], [130]. The resulting thermal stress can lead to breakage of particles into coarse or fine fragments [130]. Basu et al. stated that coal particles break into several smaller fragments resembling parent coal in size [133], while Litun et al. defined this fragmentation when intital particle disintergrates into two or multiple parts [137]. Generally, primary fragmentation follows two patterns depending on the fuel particle size and the heating rate [140]; more details of which is given in Section 4.4.1. Fragments formed during this phase are relatively coarser compared to those from attrition [134], [135]. However, particles at the smaller end of the fragment size distribution may be fine enough to be categorized as elutriable [135]. It was reported that the thermal stress resulting from pressure created during volatile evolution is larger than the mechanical stress [136]. Apart from thermal stress, particle shrinkage also contributes to primary fragmentation [107].

4.2.2 Secondary fragmentation

Secondary fragmentation, also known as char fragmentation [136], occurs during post-devolatilization combustion [133]. As the fuel burns, the internal carbon bridges of the devolatilized particle weaken [136], and is not able to withstand the hydrodynamic forces [133]. This eventually results in loss or breakage of the carbon bridges connecting the region inside fuel particle by mechanical stress, and their subsequent fragmentation [107], [135]. Contrary to primary

fragmentation which takes place only during devolatilization, secondary fragmentation happens throughout the char conversion time, and influences the particle size distribution and char surface for conversion [136]. Montagnaro et al. reported that secondary fragmentation is caused by high velocity collisions of particles with each other and with bed materials, reactor walls and grids, exit region of the riser and in cyclone of a circulating bed [130]. Again, in this phenomenon the fragments generated are larger in size than the attrited fines [130], [133].

4.2.3 Percolative fragmentation

Secondary fragmentation is succeeded by percolative fragmentation when char particles are greatly weakened during advanced phases of char conversion, or when over 50% of conversion has been completed [136]. As combustion occurs uniformly across the char body, there is sudden collapse of internal particle connectivity [133]. This is due to pore enlargement, coalescene, porosity reaching a critical value at the particle surface, and overlapping related to internal reactions [103], [107], [109]. Percolative fragmentation produces multitudes of fines ranging in the elutriable size, and whose generation rate is directly related to the carbon burning rate at the particle surface [103], [136]. Cirone et al. argued that the fine produced in this case are not elutriable but are fairly small to cause internal burning under chemical kitnetic control [134].

4.2.4 Attrition

Attrition produces fines that are elutriable [130] and are generally 90 μm or smaller in size [133]. Attrition occurs by abrasion mechanism [141] but it can be broadly divided into two categories; mechanical and combustion-assisted attrition [136]. In the former, fines are abraded from the surface of the parent particle by collisions with the bed material and the walls of reactor [107], [134]. In the latter, attrition is caused by chemical and thermal stresses [136]. Mechanical attrition is characterized by loss of ash layer while combustion-assisted generates fines in low reactive fuels

[136]. Walsh et al. has defined attrition as an abrasive wear by collisions with sorbent particles and heat transfer surface [135]. Attrition mainly impacts the fly ash and bottom ash discharges from the reactor [136].

Realizing that the last review on this topic was written 30 years ago, and various scientific studies have been published thereafter which have advanced the knowledge in this field. Therefore, this paper attempts to review the literature works concerning this topic.

4.3 Experimental set-ups presented in literature

Mainly three experiments are conducted using the same setup but in three different configurations [119], [122], [141]. They are particle fragmentation, fines elutriation rate and single particle combustion experiment.

The main apparatus consists of a stainless-steel atmospheric bubbling fluidized combustor 40 mm ID and 1 m high. A 2 mm thick perforated plate with 55 hole of 0.5 mm diameter is disposed in a triangular pitch, and acts as a fluidization gas distributor. A 0.6 m high stainless-steel column, positioned under the distributor, is filled with scrap steel to be used as a preheater. Two semi-cylindrical 2.2 kW electric furnaces are used to heat the fluidization column and the preheating section. Bed temperature is measured using chromel-alumel thermocouple located 40 mm above the distributor. The temperature is kept constant using a PID controller. The freeboard is unlagged to reduce fines post combustion. Gases are introduced to the column through two high precision digital mass flowmeters. Irrespective of the test done, the reactor was charged with 180 g of sand [122].

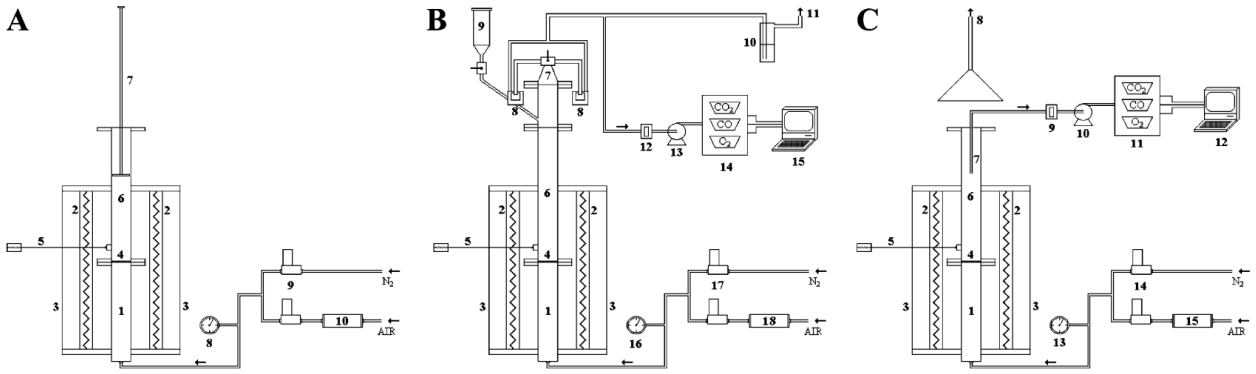

Figure 4. 2. Experimental apparatus used in literature studies. Experimental apparatus: (A) basket equipped configuration, (B) two-exit head configuration, and (C) open top configuration. (A) (1) gas preheating section, (2) electrical furnaces, (3) ceramic insulator, (4) gas distributor, (5) thermocouple, (6) fluidization column, (7) steel basket, (8) manometer, (9) digital mass flowmeters, and (10) air dehumidifier (silica gel); (B) (1) gas preheating section, (2) electrical furnaces, (3) ceramic insulator, (4) gas distributor, (5) thermocouple, (6) fluidization column, (7) head with three-way valve, (8) sintered brass filters, (9) hopper, (10) scrubber, (11) stack, (12) cellulose filter, (13) membrane pump, (14) gas analyzers, (15) personal computer, (16)manometer, (17) digital mass flowmeters, and (18) air dehumidifier (silica gel); (C) (1) gas preheating section, (2) electrical furnaces, (3) ceramic insulator, (4) gas distributor, (5) thermocouple, (6) fluidization column, (7) gas suction probe, (8) stack, (9) cellulose filter, (10) membrane pump, (11) gas analyzers, (12) personal computer, (13) manometer, (14) digital mass flowmeters, and (15) air dehumidifier (silica gel). Reproduced with permission from [122]. Copyright 2006 American Chemical Society.

4.3.1 Particle fragmentation experiment

The first configuration (Figure 4.2 A) is used for assessing primary and secondary fragmentation by particle fragmentation test. The top of the fluidization column is open to the atmosphere so that

a stainless-steel circular basket of 0.8 mm mesh size can be inserted. The mesh size allows for bed particles to pass through. The basket is used to recover fragmented and unfragmented particles from the bed. The tolerance between the column walls and the basket is kept minimum to decrease the quantity of carbon left in the bed when the basket is removed [122].

4.3.2 Fines elutriation rates experiment

The second configuration (Figure 4.2 B) is used for fines elutriation rate experiments. The top flange of the fluidization column is provided with a two-exit brass head fitted with a three-way valve. The valve can be operated to convey flue gases alternately to two removable filters of sintered brass. Batches of material can be fed to the bed through the hopper connected sideways to the upper portion of the freeboard. The online measurements of O_2, CO and CO_2 concentrations is done using a paramagnetic analyzer and two NDIR analysers in the exhaust gases [122].

4.3.3 Single particle combustion experiment

The third configuration (Figure 4.2 C) is for single particle combustion experiments. The top section of the fluidization column is left open, and a stainless-steel probe is inserted to convey fraction of exit gases to the gas analyzers. In order to prevent particle entrainment into the analyser, a high efficiency cellulose filter is used in the setup. The probe is 2 mm ID, located 0.6 m above the distributor and roughly at the axis of the column. Data from the analyser are logged and processed on a PC [122].

4.4 Comminution in a fluidized bed reactor

4.4.1 Fragmentation experiments

Primary fragmentation experiments have shown that there are dual fragmentation patterns followed during this comminution phase [26], [31]. The first one is when the parent particle breaks

into larger parts due to fractures to the center (as shown in Figure 4.1) during devolatilization, and the second is the exfoliation of the outer shell of the parent particle into smaller fragments (Figure 4.3) which occurs when the coal particle is injected into a hot atmosphere of the reactor [31]. Senneca et al. showed that the main factors that result in different primary fragmentation patterns are initial particle size, heating rate, and heating intensity [26]. When the initial size of the coal particle is large with low heating conditions, internal stress from volatile evolution prevails, and the particle gets fragmented into larger parts. Other the other hand when the particle size is small and temperature is high, finer fragments are broken from the outer particle shell due to dominating thermal stress [26], [32]. Under certain circumstances, sequential exfoliation of the shell and fragmentation of the core may occur amid intensely hot conditions for large particles [26]. Thereby, various primary fragmentation modes might occur during combustion of coal as shown in Figure 4.3 [140], [142].

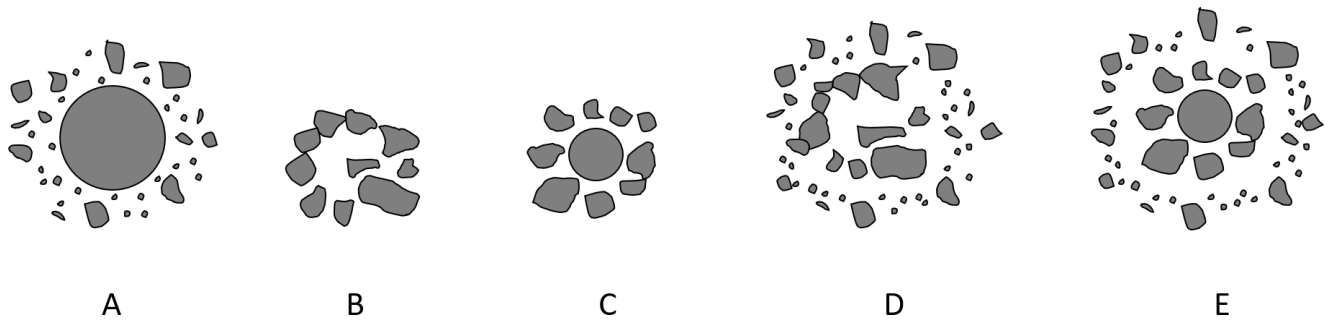

Figure 4. 3. Primary fragmentation modes of coal: (A) exfoliation; (B) fragmentation at the particle center; (C) fragmentation at internal radial position; (D) exfoliation and fragmentation at the center; (E) exfoliation and fragmentation at an internal radial position. Adapted with permission from [140]. Copyright 2013 Elsevier.

In theory, particles do not always fragment at the center. Their fragmentation also depends on the presence of pores, irregularities in shape, and non-uniformity of coal particles. Such factors determine at which position thermal stress is maximum, and if same- or uneven-sized fragments will be formed [143].

Primary and secondary fragmentation experiments are carried out by monitoring comminution factors such as multiplication factor (the number of fragments produced per unit fuel particle or char particle fed to the reactor) [119], [122], Sauter mean diameter, and fragmentation probability (the number of fuel particles undergoing primary fragmentation divided by total number of fuel particles fed) [122], [144]. Scala et al. [119] studied the comminution of biomass fuels and showed they did not undergo any substantial primary fragmentation while they presented zero to moderate secondary fragmentation. In another study Scala et al. [122] demonstrated that most biomass fuels were subject to extensive primary fragmentation represented by large multiplication factor. This led to a significant decrease in the mean diameter of the particle. It was assumed that a part of this size reduction is attributed to particle shrinkage upon devolatilization. No detectable secondary fragmentation was observed for olive husk with multiplication factor being equal to 1. While in the case of wood chips and pine seed shells, they underwent moderate fragmentation under inert conditions. The multiplication factor increased and then decrease with increase in oxygen concentrations. This observation was due to several competing factors; elutriation of small sized fragments produced by combustion mechanisms, and greater extent of char fragmentation as a result of lengthy exposure to mechanical stresses with decrease in oxygen concentration.

Primary and secondary fragmentation significantly impacts the average particle size and distribution. Thus, neglecting these two phenomena will lead to errors while evaluating actual fuel particle size in the boiler [122].

4.4.2 Elutriation rate

Various studies on coal, biomass and waste derived fuels investigated pure mechanical and combustion-assisted attrition by operating fluidized bed under inert and oxidizing conditions [121], [122], [124], [144]. These studies revealed similar trends for carbon elutriation rate. Under inert conditions, carbon elutriation rate was characterized by an initial peak in elutriation rate period due to rounding off of particle surface accompanied by a progressive decline towards an asymptotic value [121], [124]. While passing in oxidation conditions, the elutriation rate was much lower compared to purely mechanical attrition condition. Moreover, as the oxygen concentration was further increased the elutriation rate decreased. Studies show that this trend was a result of two competing phenomena [122], [124], [144]. On one hand, an increase in attrition was seen during combustion due to weakening effect of internal particle burning. On other hand, high intrinsic reactivity of attrited fines result in significant postcombustion during their residence time in bed. The enhanced attrition rate caused by combustion was counterbalanced by the extensive afterburning of fines in this case. Another study on pelletized biogenic fuels speculate that the shielding effect of ash skeleton may prevent attrition of inner layers of the pellet which brings about the decline in carbon elutriation rate under oxidizing conditions [121]. Since, the carbon fines produced by attrition are burnt off within the fluidized bed due to their high reactivity, the amount of char leaving the reactor can be considered negligible [122].

The overall effect of fines generation and their afterburning gave rise to a noticeable enhancement of coarse char combustion rate [122]. Carbon loss by elutriation is a key factor during gasification for low reactive fuels. However, fuels which show high reactivity and mechanical strength present as being favourable for achieving high carbon conversion during this process [144].

4.5 Factors affecting comminution

4.5.1 Porosity

The relatively porous structure of coal greatly influences devolatilization, char weakening and particle fragmentation during combustion [110], [145]. The explanation of how porosity impacts fragmentation is summarized by Dakič et al. [146] by relating it with volatile evolution. The extent to which volatiles move inside the coal particle is determined by the porosity of the parent coal, before a porous char is formed. The space formerly occupied by volatiles and the deformation due to pressure build up effects the resulting structure of the char. Volatiles experience stress inside the char particle due to limited transport capacity. The subsequent pressure built up leads to two scenarios; breakage of particle under strain (fragmentation), or plastic deformation to accommodate the volatiles (swelling) [146]. In other words, it is the thermal stress due to the release of volatiles which fractures the openings in the structure, forming multiple cavities during devolatilization. Thereby weakening the char structure and fragmenting the solid fuel [145]. In general, heating up of coal modifies the pore structure by devolatilization, plasticity, swelling, contraction, thermal stresses, and re-arrangement of crystal structure [110].

Study of textural structure in biomass can help to percieve the phenomenon of fragmentation. Scala et al. [122] related the porosity of wood chips, olive husk, and pine seed shells morphology with primary and secondary fragmentation. The fibrous nature of wood chips and pine seed shells fuel resulted in a char with anisotropic porous structure. Olive husk char also exhibited large pores but with irregular orientation. It was observed that larger the porosity, lower is the mechanical resistance, and thus higher the tendency of fuels to fragment. The opposite was noted for compact structured fuels which exhibit higher mechanical resistance [122].

Kosowska-Golachowska et al. [110] reported that coals with smaller porosity generated large number of fragments during devolatilization process. Low rank coals produced many fragments during combustion (secondary fragmentation) as compared to high rank coals [110]. Howewer, this observation is not in line with Sasongko et al. [111]. They explained that high porosity was exhibited by low rank coals which allows easier escape of volatiles and lesser fragments than high rank coals. The small porous structrure in high rank coals limits the flow of volatiles, and hence significant pressure is accumulated inside the particle, and tendency to fragment is higher [111]. Zhong et al. [147] also presented the explanation for this observation. Larger porosity indicates that there are several channels to faciliate smooth escape of volatile gases, and so the accumulated internal pressure is reduced. Particles which are more porous are flexible and show high thermal stress resistence. The porous structure allows enough room for heated local parts to expand freely, so there is little hinderence from peripheral solid, eventually reducing the thermal stress [147].

4.5.2 Particle size and shape

Fragmentation intensifies exponentially with increasing diameter of fuel particles. Since, larger sized coal particles posses larger quantities of volatiles, the resulting pressure generated during devolatilization will be high, and primary fragmentation will be intense [110]. Similar observation was seen in wood fuels; with increase in initial diameter, the tendency to fragment also increased [138]. Furthermore, multiplication factor is also higher for particles with large size [115]. On the other hand, coal particles with small diameter have larger specific surfaces, and so the evolution rate of volatiles is high. This leads to low inner pressure and less fragmentation [106]. Likewise, a study on coal blends revealed that fragmentation of particles with large initial diameter was more than smaller diameter particles as a consequence of reduced particle strength with size [115].

The shape of a fuel particle determines the exposed external surface area per unit mass for attrition and combustion [122]. Oblong shaped particles [138] or elongated rectangular particles [139] are more susceptible to fragmentation than quasi- circular (cubic) particle of the same diameter. This is because heating of the elongated particle will be faster volumetrically owing to the shorter distance between the surface and any central point along the longitudinal axis. Volatile evolution and accumulation will occur in the core of the particle with a shorter time delay relative to the regions near the surface. In other words, pyrolysis will take place quickly, and gas pressure will rise at a faster rate. The resulting stress due to volatile release will be higher inside the particle [126], [138].

Sphericity is the ratio of the external surface of a sphere with the same volume as the particle to the original external surface of the particle. Studies have shown that sphericity of fuel particles do not change much during devolatilization [121], [122].

4.5.3 Volatile content

Volatile content strongly influences fragmentation [106], [148]. In general, higher the content of volatile in a fuel particle, higher will be the pressure, and more immense will be the fragmentation [106]. Alternative fuels have shown to exhibit higher volatile content, which means that the devolatilization time will be extended as a consequence of greater evolution of volatiles [119]. Intensive fragmentation and attrition are observed in this case due to more fragile and porous chars developed after devolatilization of high volatile fuels [103], [119]. On the other hand, Ma et al. showed that coal blend mixed with coal slime exhibits minimum attrition due to small inner pressure from low volatile content, and showed slow rate of volatile evolution [115]. Zhong et al. explained that fragmentation in low-volatile anthracites occurs by thermal stress rather than

devolatilization as no volatile release was observed when the particles were injected into the furnace [143].

Primary fragmentation occurs as a consequence of internal stresses due to release of volatiles, provided the particle structure is not extremely porous to promote volatile escape [107]. The impact of volatile gas release and porosity of fuel on comminution is already discussed earlier in Section 4.5.1.

4.5.4 Bed temperature

Bed temperature is another factor that effects coal fragmentation [149] while it is the most influencing factor in biomass fuels [136]. With an increase in bed temperature, the heating rate increases, and the resulting inner pressure of volatiles is higher leading to an accelerated attrition rate [106], [115], [149]. In case of coal blends, the attrition rate is almost twice as high at 900^{o}C than at 800^{o}C [115]. Studies have shown that increasing the process temperature (800 - 900^{o}C) intensifies fragmentation of wood particles [126], [138].

Particles larger in size fragment more at higher temperature (950^{o}C) than at lower temperature (800^{o}C) [136]. This is because higher temperature leads to higher heating rate while larger particle size means larger temperature gradient inside the fuel particles. Both these conditions bring about greater thermal stress and greater probability of fragmentation. Regardless of high heating rate for smaller particle, the temperature gradient and thermal stress is small. Therefore, they fragment less extensively [147]. Usually large thermal stress at elevated bed temperatures promote fragmentation [115], [136].

It is seen that the number of fine particles increases with increase in devolatilization and combustion temperature. This may be because of rise in thermal stress in early stages of

devolatilization and during combustion [145]. Elutriation tendency is much higher for limestones at increased temperatures due to weakening of particle structure by vigorous generation of CO_2 [130].

Depending on the type of material in the fluidized bed reactor, different temperature ranges can affect the smoothness of the particle surface undergoing fragmentation, as in case of limestone [131]. Under 850ºC, the surface of limestone was observed to be smoother due to inter-particle collisions. However, at a temperature of 900ºC, it was seen that contrary to the smooth surface that is expected to occur due to further collisions, the surface was actually rough. It was explained that fines generated at this temperature adhered to the particle with larger surface. Limestone at high temperatures becomes adhesive leading to agglomeration of fines to its surface [131]. Table 4.3 presents a summary of all the factors affecting particle comminution.

Table 4. 3. Different factors of fuel particle effecting comminution.

Factor	Effect on comminution	Type of Fuel	Bed Temperature	Reason/mechanism	References
Porosity	Comminution is increased when porosity is high	Biomass (wood chips, pine seed shells and olive husk)	850°C	Mechanical resistance is low	[122]
	Comminution is increased when porosity is low	Coal	700-1600°C	Thermal stress resistance is high	[110], [111], [147]
Particle Morphology	Comminution is increased when particle diameter is large	Coal, and coal blend, wood biomass	700-950°C	Internal pressure and devolatilization is high	[106], [110], [115], [138], [139]

	Comminution is increased for oblong shaped particles	Biomass (wood chips, pine seed shells and olive husk), and wood biomass	800 –950°C	Devolatilization is faster due to the unique shape	[115], [122], [126], [138], [139]
Volatiles	Comminution is increased when volatile content is high	Biomass (Robinia Pseudoacacia), coal, coal blend and alternative solid fuels (biomass, agricultural, civil and industrial wastes),	800–900°C	Internal pressure and devolatilization is high	[103], [106], [115], [119]
Temperature	Comminution is increased when bed temperature is high	Coal and coal blend	700–900°C	Heating rate and devolatilization is high	[106], [115], [149]

4.6 Initial particle size analysis during fluidized bed comminution

4.6.1 Initial particle size versus fragmentation probability

Fragmentation is more likely with an increase in initial particle size for coal and biomass with coal having a very high chance to fragment as particle size increases [136]. For particles with a mean diameter of 22.5 mm fragmentation was more prone to occur than particles with a mean diameter of 14.25 and 9 mm for coal [136]. As with biomass it was found that particles with a mean diameter of 20 mm fragment more than particles of a mean diameter of 15 mm and 10mm [136]. In numerous studies [134], [150], [151], fragment count was found to be greater as initial particle size increased as the multiplication factor increased for increased initial particle size [106]. In other words, the chances of fragmentation is much higher when the particle size is increased [136]. If the bed temperature is raised there are more chances of fragmentation irrespective of particle size due to an increase of inner pressure and thermal stress, but larger particles are still most likely to fragment for both coal and biomass [106], [136]. Figure 4.4 shows the likelihood of fragmentation as particle size increases for two different types of coal [106]. Similar, results were found for fast pyrolysis as with a larger initial diameter there was an increased the chance of fragmentation [152].

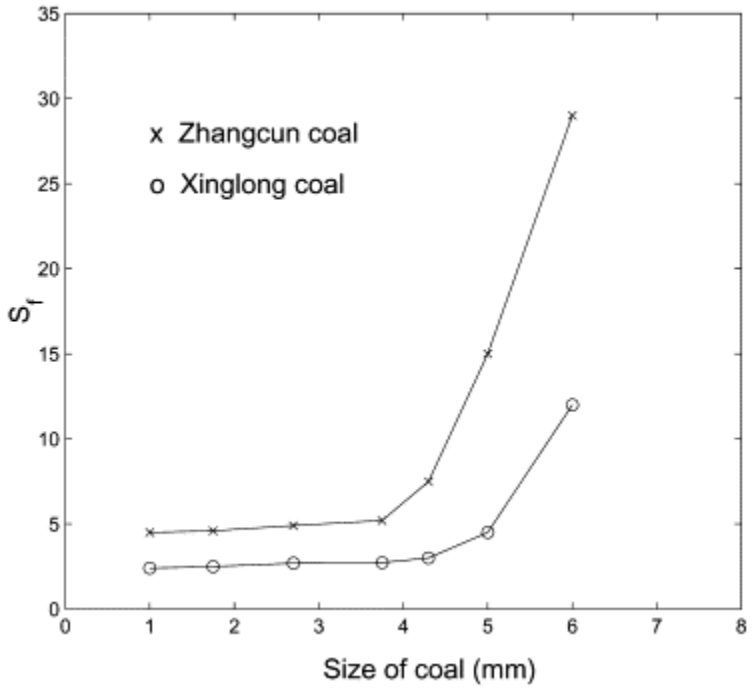

Figure 4. 4. Coal size (mm) versus fragmentation index. Reproduced with permission from [106]. Copyright 2002 Elsevier.

4.6.2 Initial particle size versus average particle size after de-volatilization

The particle size after devolatilization is dependent on initial fragment size and bed temperature with an increase in fragment size creating more fragmentations that are smaller than the original particle [136]. For particles with a mean diameter of 22.5 mm, the larger particles at the end of the process was found to be 35% of the initial size which is the greatest change in mean diameter for the three particle sizes investigated (9 mm 50% in size and 14.25 mm 40% in size) for coal [136]. In a study by Blaszczuk and Nowak, the final mean particle size ranged from 0.219 – 0.411 mm even for large fragments of 20 mm, showing that most of the particle's fragment with a major reduction in size [153]. A reduction in particle size by a factor of 0.75 was also found for small wood pellets (350 μm) and a particle size reduction of 0.6 for slightly larger wood pellets (500, 700 and 800 μm) after devolatilization [154]. Cui et al. also found a reduction in particle size for

particles as small as 122 μm. However, they noticed swelling at the start of the reaction that would slightly increase particle size, especially at low temperatures [152]. Even with the swelling there was always a reduction in size for the overall reaction for reaction times greater than 150 ms [152]. The reduction in size for both large and small initial particles show that devolatilization has a significant effect on both particles, and that this reduction must always be investigated even for small particles [137]. Coal particles were found to lose mass very quickly at high temperatures with some types of coal losing greater than 45% of their mass in just 250 ms [152].

4.6.3 Quantitative predictions of particle size distribution inside a bed

Particle size reduces as particles move through the bed with larger particles losing significant diameter through the first quarter of the residence time and losing more than 50 % by the final quarter [136]. Coal particles throughout the bed can range from 0.02 mm to 20 mm depending on the initial size of the particles [153]. Paprika et al. predicted that the diameter most common post reaction is about 1.7 mm for a coal particle that started off with a diameter between 6 – 8 mm. They ran the simulation at 850 °C and found that there were less course particles within the smaller particles [155]. Cui et al. found that coal particles between 30 – 60 μm were likely to stick to the reactor walls than smaller particles. Furthermore, they observed that the distribution of particle size was mostly constituted course particles greater than 60 μm and a small fraction of small particles less than 20 μm [152]. In a study by Pragadeesh et al. both coal and biomass saw a significant reduction in size through each quarter of the reactor bed especially for greater initial particle size. The coal particles were nearly 50% reduced halfway through the reactor bed whereas biomass produced fines 2 mm larger than their 20 mm initial size halfway through the reactor bed [136]. Thus, coal particles are more likely to reduce in size throughout the reactor bed length, but biomass sees most of its size reduction halfway through the reactor bed [136].

4.7 Conclusions

Comminution of carbon-based fuels is an important phenomenon that occurs in fluidized bed reactor. It involves a series of events, namely primary fragmentation, secondary fragmentation, percolative fragmentation, and attrition. These events considerably influence the particle size and distribution. Therefore, it is imperative to not neglect comminution to avoid oversights in actual fuel particle size evaluation in the reactor. The generation of fines and their subsequent afterburning results in an enhanced coarse char combustion rate. Elutriation is a crucial factor in low reactive fuels as it leads to carbon loss. While the carbon fines generated by attrition are consumed within the bed by combustion due to their high reactivity. It is, therefore, safe to neglect the amount of char escaping in this case. Porosity, particle size, volatile content, and bed temperature are some of the key factors that influence comminution.

Chapter 5
Conclusions and Recommendations

5.1 Conclusions

The urgent need for sustainable energy solutions due to increasing carbon dioxide emissions from fossil fuel combustion highlights hydrogen's potential as a CO_2-neutral option. Microwave pyrolysis of methane, a promising method, exclusively produces solid carbon and hydrogen gas, avoiding CO_2 by-products. This method involves radiating microwaves on seed carbon (SC); an activated carbon; as a microwave receptor which heats and convert methane into pure hydrogen gas and solid carbon. The solid carbon generated, known as product carbon (PC), continues to act as a microwave receptor and sustains the process of methane pyrolysis. Permittivity studies were conducted on the carbon samples which confirmed that microwave heating efficiently permeates and heats both samples. PC exhibited varying permittivity levels while consistently maintaining overall values. Though SC was found to be more responsive to microwaves, its potential for thermal runaway is a concern. XRD analysis shows both SC and PC have amorphous structures, with PC displaying some graphitization. The carbon produced through methane pyrolysis is self-sustaining and can serve as the exclusive microwave carrier without requiring additional fresh seed carbon. This thesis presents fundamental insights onto how the PC formed can work as a microwave heat carrier for methane gas thereby making the hydrogen generation process inexpensive.

During the methane pyrolysis, fluidization of carbon, either SC or PC, is anticipated to occur which may lead to attrition of the carbon particles. In this regard, the thesis also presents an in-depth review of the different comminution phenomena that occur in a fluidized bed reactor.

The push for decarbonization is generating significant momentum across various industry sectors towards adopting cleaner energy sources. Hydrogen is identified as a promising candidate, not only for supplying energy but also for mitigating emissions. However, for hydrogen to truly contribute to decarbonization, it must be produced in an environmentally friendly manner- meaning the carbon dioxide emitted during production needs to be captured and stored, and the electricity used in the process should be sourced from clean energy. Presently, water electrolysis stands out as the most prevalent and environmentally friendly method for hydrogen production. However, the current industrial practices involve using electrodes made from precious metals like iridium, making the process technically feasible but not economically viable. In contrast, microwave methane pyrolysis, while still at a smaller scale, offers a promising alternative. This method produces solid carbon as a byproduct, effectively removing CO_2 from the equation. The resulting solid carbon also functions as a heat carrier for methane gas, making the process more cost-effective compared to water electrolysis. Although tested on a small scale, this technology holds promise for hydrogen production in a very economic fashion- subjected to methane availability and clean source of electricity.

5.2 Recommendations

- The tests conducted at the lab scale have provided valuable insights, but to assess the true performance, it is necessary to replicate the experiments in realistic atmospheres.
- The carbon produced through microwave pyrolysis shows promise for application in various fields such as steelmaking, graphene production, anode material in Na-ion batteries, etc. therefore it should be tested for these applications.

- To gain a comprehensive understanding of the economic viability, a technoeconomic analysis comparing heat supplied by microwaves with conventional heating methods is essential.
- Conducting a life cycle assessment (LCA) of the electricity used to generate microwaves will help evaluate the environmental impact of this heating approach.
- Further investigation is required to explore the influence of particle size on heating efficiency. Study of comminution exclusively inside the pyrolysis reactor due to fluidization is required to completely understand how particle size affects the microwave absorption and heat generation process can optimize the design of the pyrolysis system.
- Blending natural gas with other industrial gases may have an impact on the carbon performance efficiency. Investigating this aspect will shed light on potential improvements in the carbon production process by fine-tuning gas compositions.
- Examining and optimizing the quantity of carbon fed and produced within the pyrolysis reactor is required to elucidate its influence on microwave absorption and the overall efficiency of the entire process.

By pursuing these investigations, we can enhance the efficiency and effectiveness of microwave pyrolysis of methane and its applications, making progress towards a more sustainable and cost-effective energy solution.

References

[1] M. Jasiński, M. Dors, H. Nowakowska, and J. Mizeraczyk, "Hydrogen production via methane reforming using various microwave plasma sources," *Chemicke Listy*, vol. 102, p. s1332−s1337, 2008.

[2] C. M. Kalamaras and A. M. Efstathiou, "Hydrogen Production Technologies : Current State and Future Developments," *Energy*, vol. 2013, 2013.

[3] L. García, *Hydrogen production by steam reforming of natural gas and other nonrenewable feedstocks*. Elsevier Ltd, 2015. doi: 10.1016/B978-1-78242-361-4.00004-2.

[4] J. D. Holladay, J. Hu, D. L. King, and Y. Wang, "An overview of hydrogen production technologies," *Catalyst Today*, vol. 139, pp. 244–260, 2009, doi: 10.1016/j.cattod.2008.08.039.

[5] D. H. Lee, *Hydrogen production via the Kværner process and plasma reforming*. 2015. doi: 10.1016/B978-1-78242-361-4.00012-1.

[6] R. Cassia, M. Nocioni, N. Correa-Aragunde, and L. Lamattina, "Climate change and the impact of greenhouse gasses: CO2 and NO, friends and foes of plant oxidative stress," *Front Plant Sci*, vol. 9, pp. 1–11, 2018, doi: 10.3389/fpls.2018.00273.

[7] T. Gentzis, "Subsurface sequestration of carbon dioxide - an overview from an Alberta (Canada) perspective," *Int J Coal Geol*, vol. 43, pp. 287–305, 2000, doi: 10.1016/S0166-5162(99)00064-6.

[8] M. Shaygan, M. A. Ehyaei, A. Ahmadi, M. E. H. Assad, and J. L. Silveira, "Energy, exergy, advanced exergy and economic analyses of hybrid polymer electrolyte membrane (PEM)

fuel cell and photovoltaic cells to produce hydrogen and electricity," *J Clean Prod*, vol. 234, pp. 1082–1093, 2019, doi: 10.1016/j.jclepro.2019.06.298.

[9] S. Iglauer, M. Ali, and A. Keshavarz, "Hydrogen Wettability of Sandstone Reservoirs: Implications for Hydrogen Geo-Storage," *Geophys Res Lett*, vol. 48, no. 3, 2021, doi: 10.1029/2020GL090814.

[10] B. J. Leal Pérez, J. A. Medrano Jiménez, R. Bhardwaj, E. Goetheer, M. van Sint Annaland, and F. Gallucci, "Methane pyrolysis in a molten gallium bubble column reactor for sustainable hydrogen production: Proof of concept & techno-economic assessment," *Int J Hydrogen Energy*, vol. 46, pp. 4917–4935, 2021, doi: 10.1016/j.ijhydene.2020.11.079.

[11] A. Konieczny, K. Mondal, T. Wiltowski, and P. Dydo, "Catalyst development for thermocatalytic decomposition of methane to hydrogen," *International Journal of Hydogen Engergy*, vol. 33, pp. 264–272, 2008, doi: 10.1016/j.ijhydene.2007.07.054.

[12] L. Gonzalez Marciaga, "Assessment of usage of hydrogen as alternative fuel into NETPLAN," Iowa State University, 2013.

[13] S. Dutta, "A review on production , storage of hydrogen and its utilization as an energy resource," *Journal of Industrial and Engineering Chemistry*, vol. 20, no. 4, pp. 1148–1156, 2014, doi: 10.1016/j.jiec.2013.07.037.

[14] M. Dadsetan *et al.*, "Characterization of carbon products from microwave-driven methane pyrolysis," *Carbon Trends*, vol. 12, Sep. 2023, doi: 10.1016/j.cartre.2023.100277.

[15] M. Dadsetan, M. F. Khan, M. Salakhi, E. R. Bobicki, and M. J. Thomson, “CO2-free hydrogen production via microwave-driven methane pyrolysis,” *Int J Hydrogen Energy*, vol. 48, no. 39, pp. 14565–14576, May 2023, doi: 10.1016/j.ijhydene.2022.12.353.

[16] S. Schneider, S. Bajohr, F. Graf, and T. Kolb, “State of the art of hydrogen production via pyrolysis of natural gas,” *ChemBioEng Reviews*, vol. 7, no. 5, pp. 150–158, 2020, doi: 10.1002/cben.202000014.

[17] N. Z. Muradov and T. N. Veziroğlu, “From hydrocarbon to hydrogen-carbon to hydrogen economy,” *Int J Hydrogen Energy*, vol. 30, no. 3, pp. 225–237, Mar. 2005, doi: 10.1016/j.ijhydene.2004.03.033.

[18] A. Abánades *et al.*, “Experimental analysis of direct thermal methane cracking,” *Int J Hydrogen Energy*, vol. 36, no. 20, pp. 12877–12886, Oct. 2011, doi: 10.1016/j.ijhydene.2011.07.081.

[19] B. Fidalgo, Y. Fernández, A. Domínguez, J. J. Pis, and J. A. Menéndez, “Microwave-assisted pyrolysis of CH4/N2 mixtures over activated carbon,” *J Anal Appl Pyrolysis*, vol. 82, no. 1, pp. 158–162, 2008, doi: 10.1016/j.jaap.2008.03.004.

[20] D. O. Cooney and Z. Xi, “Production of hydrogen from methane and methane/steam in a microwave irradiated char-loaded reactor,” *Fuel Science and Technology International*, vol. 14, no. 8, pp. 1111–1141, 1996, doi: 10.1080/08843759608947631.

[21] F. Motasemi and M. T. Afzal, “A review on the microwave-assisted pyrolysis technique,” *Renewable and Sustainable Energy Reviews*, vol. 28, pp. 317–330, 2013, doi: 10.1016/j.rser.2013.08.008.

[22] A. Domínguez, B. Fidalgo, Y. Fernández, J. J. Pis, and J. A. Menéndez, "Microwave-assisted catalytic decomposition of methane over activated carbon for CO2-free hydrogen production," *Int J Hydrogen Energy*, vol. 32, no. 18, pp. 4792–4799, 2007, doi: 10.1016/j.ijhydene.2007.07.041.

[23] K. Juda, B. A. Glowacki, K. L. Juda, A. Clayton, and B. A. Glowacki, "The influence of microwave plasma power on the degree of natural gas conversion to carbon nanoforms," in *2nd Global Congress on Microwave Energy Applications*, 2012. doi: 10.13140/RG.2.1.2668.2328.

[24] Y. D. Korolev *et al.*, "Nonself-sustained microwave discharge in a system for hydrocarbon decomposition and generation of carbon nanotubes," in *IEEE Transactions on Plasma Science*, Dec. 2009, pp. 2298–2302. doi: 10.1109/TPS.2009.2032546.

[25] J. Medvedev, "2317943C2," 2006

[26] S. I. Galanov, A. G. Zherlitsyn, Yu. V Medvedev, O. I. Sidorova, and V. P. Shiyan, "Production of a highly dispersed carbon material and hydrogen from natural gas in a microwave reactor with metallic catalysts," *Russian Journal of Applied Chemistry*, vol. 84, no. 6, pp. 997–1002, 2011, doi: 10.1134/S1070427211060176.

[27] A. G. Zherlitsyn, V. P. Shiyan, and P. V. Demchenko, "Microwave plasma torch for processing hydrocarbon gases," *Resource-Efficient Technologies*, vol. 2, no. 1, pp. 11–14, Mar. 2016, doi: 10.1016/j.reffit.2016.04.001.

[28] X. Zeng *et al.*, "Growth and morphology of carbon nanostructures by microwave-assisted pyrolysis of methane," *Physica E Low Dimens Syst Nanostruct*, vol. 42, no. 8, pp. 2103–2108, Jun. 2010, doi: 10.1016/j.physe.2010.04.002.

[29] T. Kim, J. Lee, and K. H. Lee, "Microwave heating of carbon-based solid materials," *Carbon Letters*, vol. 15, no. 1, pp. 15–24, 2014, doi: 10.5714/CL.2014.15.1.015.

[30] E. R. Bobicki, C. A. Pickles, J. Forster, O. Marzoughi, and R. Hutcheon, "High temperature permittivity measurements of selected industrially relevant ores: Review and analysis," *Miner Eng*, vol. 145, no. September 2019, p. 106055, 2020, doi: 10.1016/j.mineng.2019.106055.

[31] N. Devi, S. Sahoo, R. Kumar, and R. K. Singh, "A review of the microwave-assisted synthesis of carbon nanomaterials, metal oxides/hydroxides and their composites for energy storage applications," *Nanoscale*, vol. 13, no. 27, pp. 11679–11711, Jul. 2021, doi: 10.1039/d1nr01134k.

[32] J. A. Menéndez *et al.*, "Microwave heating processes involving carbon materials," *Fuel Processing Technology*, vol. 91, no. 1, pp. 1–8, 2010, doi: 10.1016/j.fuproc.2009.08.021.

[33] M. Gupta and W. L. Wong, *Microwaves and Metals*. John Wiley & Sons, 2007.

[34] P. A. Mello, J. S. Barin, and R. A. Guarnieri, "Microwave Heating," in *Microwave-Assisted Sample Preparation for Trace Element Determination*, Elsevier B.V., 2014, pp. 59–75. doi: 10.1016/B978-0-444-59420-4.00002-7.

[35] M. Gupta and E. Wong Wai Leong, "Microwaves – Theory," in *Microwaves and Metals*, 2007, pp. 25–41. doi: https://doi.org/10.1002/9780470822746.ch2.

[36] Z. Wang, C. Yu, H. Huang, W. Guo, J. Yu, and J. Qiu, “Carbon-enabled microwave chemistry: From interaction mechanisms to nanomaterial manufacturing,” *Nano Energy*, vol. 85, no. January, p. 106027, 2021, doi: 10.1016/j.nanoen.2021.106027.

[37] A. C. Metaxas and R. J. (Roger J.) Meredith, *Industrial microwave heating*. P. Peregrinus on behalf of the Institution of Electrical Engineers, 1983.

[38] C. A. Pickles, E. R. Bobicki, O. Marzoughi, J. Forster, D. Boucher, and R. Hutcheon, “Temperature, frequency and compositional dependencies of the permittivities of hydroxide minerals,” *Miner Eng*, vol. 174, no. December 2020, p. 107244, 2021, doi: 10.1016/j.mineng.2021.107244.

[39] S. Marland, A. Merchant, and N. Rowson, “Dielectric properties of coal,” *Fuel*, vol. 80, no. 13, pp. 1839–1849, 2001.

[40] F. Motasemi, A. A. Salema, and M. T. Afzal, “Dielectric characterization of corn stover for microwave processing technology,” *Fuel Processing Technology*, vol. 131, pp. 370–375, 2015, doi: 10.1016/j.fuproc.2014.12.006.

[41] J. Sun, W. Wang, and Q. Yue, “Review on microwave-matter interaction fundamentals and efficient microwave-associated heating strategies,” *Materials*, vol. 9, no. 4. MDPI AG, 2016. doi: 10.3390/ma9040231.

[42] F. Mushtaq, R. Mat, and F. N. Ani, “A review on microwave assisted pyrolysis of coal and biomass for fuel production,” *Renewable and Sustainable Energy Reviews*, vol. 39, pp. 555–574, 2014, doi: 10.1016/j.rser.2014.07.073.

[43] J.-K. Yang and Y.-M. Wu, “Relation between dielectric property and desulphurization of coal by microwaves,” *Fuel*, vol. 66, no. 12, pp. 1745–1747, 1987.

[44] Z. Fang, C. Li, J. Sun, H. Zhang, and J. Zhang, “The electromagnetic characteristics of carbon foams,” *Carbon N Y*, vol. 45, no. 15, pp. 2873–2879, 2007.

[45] K. H. Wu, T. H. Ting, G. P. Wang, C. C. Yang, and C. W. Tsai, “Synthesis and microwave electromagnetic characteristics of bamboo charcoal/polyaniline composites in 2–40 GHz,” *Synth Met*, vol. 158, no. 17–18, pp. 688–694, 2008.

[46] S. Challa, W. E. Little, and C. Y. Cha, “Measurement of the dielectric properties of char at 2.45 GHz,” *Journal of Microwave Power and Electromagnetic Energy*, vol. 29, no. 3, pp. 131–137, 1994.

[47] J. E. Atwater and R. R. Wheeler, “Temperature dependent complex permittivities of graphitized carbon blacks at microwave frequencies between 0.2 and 26 GHz,” *J Mater Sci*, vol. 39, pp. 151–157, 2004.

[48] J. Ma, M. Fang, P. Li, B. Zhu, X. Lu, and N. T. Lau, “Microwave-assisted catalytic combustion of diesel soot,” *Appl Catal A Gen*, vol. 159, no. 1–2, pp. 211–228, 1997.

[49] J. E. Atwater and J. Wheeler RR, “Microwave permittivity and dielectric relaxation of a high surface area activated carbon,” *Applied Physics A*, vol. 79, pp. 125–129, 2004.

[50] J. E. Atwater and R. R. Wheeler Jr, “Complex permittivities and dielectric relaxation of granular activated carbons at microwave frequencies between 0.2 and 26 GHz,” *Carbon N Y*, vol. 41, no. 9, pp. 1801–1807, 2003.

[51] E. A. Dawson, G. M. B. Parkes, P. A. Barnes, G. Bond, and R. Mao, "The generation of microwave-induced plasma in granular active carbons under fluidised bed conditions," *Carbon N Y*, vol. 46, no. 2, pp. 220–228, 2008.

[52] H. Lin, H. Zhu, H. Guo, and L. Yu, "Microwave-absorbing properties of Co-filled carbon nanotubes," *Mater Res Bull*, vol. 43, no. 10, pp. 2697–2702, 2008.

[53] L. Zhang and H. Zhu, "Dielectric, magnetic, and microwave absorbing properties of multi-walled carbon nanotubes filled with Sm2O3 nanoparticles," *Mater Lett*, vol. 63, no. 2, pp. 272–274, 2009.

[54] Y. Yao, A. Jänis, and U. Klement, "Characterization and dielectric properties of β-SiC nanofibres," *J Mater Sci*, vol. 43, pp. 1094–1101, 2008.

[55] T. Kim, J. Lee, and K. H. Lee, "Full graphitization of amorphous carbon by microwave heating," *RSC Adv*, vol. 6, no. 29, pp. 24667–24674, 2016, doi: 10.1039/c6ra01989g.

[56] N. Bundaleska *et al.*, "Microwave plasma enabled synthesis of free standing carbon nanostructures at atmospheric pressure conditions," *Physical Chemistry Chemical Physics*, vol. 20, no. 20, pp. 13810–13824, 2018.

[57] J. Ge *et al.*, "Joule-heated graphene-wrapped sponge enables fast clean-up of viscous crude-oil spill," *Nat Nanotechnol*, vol. 12, no. 5, pp. 434–440, 2017.

[58] A. Zlotorzynski, "The application of microwave radiation to analytical and environmental chemistry," *Crit Rev Anal Chem*, vol. 25, no. 1, pp. 43–76, 1995.

[59] R. J. Meredith, *Engineers' handbook of industrial microwave heating*, no. 25. Iet, 1998.

[60] D. A. Jones, T. P. Lelyveld, S. D. Mavrofidis, S. W. Kingman, and N. J. Miles, "Microwave heating applications in environmental engineering—a review," *Resour Conserv Recycl*, vol. 34, no. 2, pp. 75–90, 2002.

[61] A. Zlotorzynski, "The application of microwave radiation to analytical and environmental chemistry," *Crit Rev Anal Chem*, vol. 25, no. 1, pp. 43–76, 1995.

[62] A. Dominguez *et al.*, "Conventional and microwave induced pyrolysis of coffee hulls for the production of a hydrogen rich fuel gas," *J Anal Appl Pyrolysis*, vol. 79, no. 1–2, pp. 128–135, 2007.

[63] Y. Fernández, A. Arenillas, M. A. Díez, J. J. Pis, and J. A. Menéndez, "Pyrolysis of glycerol over activated carbons for syngas production," *J Anal Appl Pyrolysis*, vol. 84, no. 2, pp. 145–150, 2009.

[64] P. Monsef-Mirzai, M. Ravindran, W. R. McWhinnie, and P. Burchil, "The use of microwave heating for the pyrolysis of coal via inorganic receptors of microwave energy," *Fuel*, vol. 71, no. 6, pp. 716–717, 1992.

[65] L. Xu and H. K. Lee, "Novel approach to microwave-assisted extraction and micro-solid-phase extraction from soil using graphite fibers as sorbent," *J Chromatogr A*, vol. 1192, no. 2, pp. 203–207, 2008.

[66] D. Li, X. Quan, Y. Zhang, and Y. Zhao, "Microwave-induced thermal treatment of petroleum hydrocarbon-contaminated soil," *Soil Sediment Contam*, vol. 17, no. 5, pp. 486–496, 2008.

[67] M. Dadsetan *et al.*, “Carbon film produced from microwave-driven methane pyrolysis,” *Carbon Trends*, vol. 12, p. 100283, Sep. 2023, doi: 10.1016/j.cartre.2023.100283.

[68] M. Dadsetan *et al.*, “Characterization of carbon products from microwave-driven methane pyrolysis,” *Carbon Trends*, vol. 12, p. 100277, Sep. 2023, doi: 10.1016/j.cartre.2023.100277.

[69] R. Hutcheon, M. DE Jong, F. Adams, P. Lucuta, J. McGREGOR, and L. Bahen, “RF and Microwave Dielectric Measurement to 1400°C and Dielectric Loss Mechanisms,” in *Mat. Res. Soc. Symp. Proc*, @1992 Materials Research Society, 1992, p. 541.

[70] R. Hutcheon, M. de Jong, F. Adams, G. Wood, J. McGregor, and B. Smith, “A System for Rapid Measurements of RF and Microwave Properties Up to 1400°C. Part 2: Description of Apparatus, Data Collection Techniques and Measurements on Selected Materials.,” *Journal of Microwave Power and Electromagnetic Energy*, vol. 27, no. 2, pp. 93–102, Jan. 1992, doi: 10.1080/08327823.1992.11688177.

[71] C. A. Pickles and O. Marzoughi, “Temperature and frequency dependencies of the permittivities of nickeliferous silicate laterite ores and reaction mixtures,” *Powder Technol*, vol. 428, p. 118867, Oct. 2023, doi: 10.1016/j.powtec.2023.118867.

[72] S. Zhang *et al.*, “Structural order evaluation and structural evolution of coal derived natural graphite during graphitization,” *Carbon N Y*, vol. 157, pp. 714–723, Feb. 2020, doi: 10.1016/j.carbon.2019.10.104.

[73] J. Biscoe and B. E. Warren, “An x-ray study of carbon black,” *J Appl Phys*, vol. 13, no. 6, pp. 364–371, 1942, doi: 10.1063/1.1714879.

[74] Z. Peng, J.-Y. Hwang, W. Bell, M. Andriese, and S. Xie, “Microwave dielectric properties of pyrolyzed carbon,” 2011.

[75] A. Ibrahim *et al.*, “Preparation and characterization of activated carbon obtained from Melaleuca cajuputi leaves,” *Carbon Trends*, vol. 13, Dec. 2023, doi: 10.1016/j.cartre.2023.100301.

[76] T. Zhang, X. Zhang, and H. Li, “Kinetics and equilibrium study of phenol adsorption by activated carbon derived from pig blood,” *Carbon Trends*, vol. 12, Sep. 2023, doi: 10.1016/j.cartre.2023.100281.

[77] D. Cuhadaroglu and O. A. Uygun, “Production and characterization of activated carbon from a bituminous coal by chemical activation,” *Afr J Biotechnol*, vol. 7, no. 20, pp. 3703–3710, 2008, [Online]. Available: http://www.academicjournals.org/AJB

[78] C. A. Pickles, F. Gao, and S. Kelebek, “Microwave drying of a low-rank sub-bituminous coal,” *Miner Eng*, vol. 62, pp. 31–42, 2014, doi: 10.1016/j.mineng.2013.10.011.

[79] S. O. Nelson, G. E. Fanslow, and D. D. Bluhm, “Frequency dependence of the dielectric properties of coal,” *Journal of Microwave Power*, vol. 15, no. 4, pp. 277–282, 1980.

[80] A. A. Salema, Y. K. Yeow, K. Ishaque, F. N. Ani, M. T. Afzal, and A. Hassan, “Dielectric properties and microwave heating of oil palm biomass and biochar,” *Ind Crops Prod*, vol. 50, pp. 366–374, Jan. 2013, doi: 10.1016/j.indcrop.2013.08.007.

[81] N. Alias and M. A. A. Zaini, “On the view of dielectric properties in microwave-assisted activated carbon preparation,” *Asia-Pacific Journal of Chemical Engineering*, vol. 10, no. 6, pp. 953–960, Nov. 2015, doi: 10.1002/apj.1927.

[82] C. A. Pickles, “Microwaves in extractive metallurgy: Part 1 - Review of fundamentals,” *Miner Eng*, vol. 22, no. 13, pp. 1102–1111, Oct. 2009, doi: 10.1016/j.mineng.2009.02.015.

[83] J. Forster, Y. Maham, and E. R. Bobicki, “Microwave heating of magnesium silicate minerals,” *Powder Technol*, vol. 339, pp. 1–7, Nov. 2018, doi: 10.1016/j.powtec.2018.07.069.

[84] Y. bin Tang, Q. Liu, and F. yan Chen, “Preparation and characterization of activated carbon from waste ramulus mori,” *Chemical Engineering Journal*, vol. 203, pp. 19–24, Sep. 2012, doi: 10.1016/j.cej.2012.07.007.

[85] Z.-Y. Wu *et al.*, “Non-iridium-based electrocatalyst for durable acidic oxygen evolution reaction in proton exchange membrane water electrolysis,” *Nat Mater*, vol. 22, no. 1, pp. 100–108, 2023, doi: 10.1038/s41563-022-01380-5.

[86] F. Hegge *et al.*, “Efficient and Stable Low Iridium Loaded Anodes for PEM Water Electrolysis Made Possible by Nanofiber Interlayers,” *ACS Appl Energy Mater*, vol. 3, no. 9, pp. 8276–8284, Sep. 2020, doi: 10.1021/acsaem.0c00735.

[87] M. B. Burkholder *et al.*, “Metal supported graphene catalysis: A review on the benefits of nanoparticular supported specialty sp 2 carbon catalysts on enhancing the activities of multiple chemical transformations,” *Carbon Trends*, vol. 9, p. 100196, 2022, doi: 10.1016/j.cartre.2022.100196.

[88] G. Nassar, E. Daou, R. Najjar, M. Bassil, and R. Habchi, “A review on the current research on graphene-based aerogels and their applications,” *Carbon Trends*, vol. 4, p. 100065, Jul. 2021, doi: 10.1016/J.CARTRE.2021.100065.

[89] M. Kurian and A. Paul, “Recent trends in the use of green sources for carbon dot synthesis–A short review,” *Carbon Trends*, vol. 3, p. 100032, Apr. 2021, doi: 10.1016/J.CARTRE.2021.100032.

[90] D. Ozyurt, M. Al Kobaisi, R. K. Hocking, and B. Fox, “Properties, synthesis, and applications of carbon dots: A review,” *Carbon Trends*, vol. 12, p. 100276, Sep. 2023, doi: 10.1016/J.CARTRE.2023.100276.

[91] Y. F. Huang, P. Te Chiueh, and S. L. Lo, “A review on microwave pyrolysis of lignocellulosic biomass,” *Sustainable Environment Research*, vol. 26, no. 3. Chinese Institute of Environmental Engineering, pp. 103–109, May 01, 2016. doi: 10.1016/j.serj.2016.04.012.

[92] S. S. Lam and H. A. Chase, “A review on waste to energy processes using microwave pyrolysis,” *Energies*, vol. 5, no. 10. MDPI AG, pp. 4209–4232, 2012. doi: 10.3390/en5104209.

[93] R. Moliner, I. Suelves, M. J. Lázaro, and O. Moreno, “Thermocatalytic decomposition of methane over activated carbons: influence of textural properties and surface chemistry,” *Int J Hydrogen Energy*, vol. 30, no. 3, pp. 293–300, 2005.

[94] M. J. Lázaro, J. L. Pinilla, I. Suelves, and R. Moliner, “Study of the deactivation mechanism of carbon blacks used in methane decomposition,” *Int J Hydrogen Energy*, vol. 33, no. 15, pp. 4104–4111, 2008.

[95] J. L. Pinilla, I. Suelves, M. J. Lázaro, and R. Moliner, "Kinetic study of the thermal decomposition of methane using carbonaceous catalysts," *Chemical Engineering Journal*, vol. 138, no. 1–3, pp. 301–306, 2008.

[96] N. Sánchez-Bastardo, R. Schlögl, and H. Ruland, "Methane Pyrolysis for CO2-Free H2 Production: A Green Process to Overcome Renewable Energies Unsteadiness," *Chemie Ingenieur Technik*, vol. 92, no. 10, pp. 1596–1609, Oct. 2020, doi: 10.1002/CITE.202000029.

[97] U. P. M. Ashik, W. M. A. Wan Daud, and H. F. Abbas, "Production of greenhouse gas free hydrogen by thermocatalytic decomposition of methane – A review," *Renewable and Sustainable Energy Reviews*, vol. 44, pp. 221–256, Apr. 2015, doi: 10.1016/J.RSER.2014.12.025.

[98] J. Zhang, X. Li, W. Xie, Q. Hao, H. Chen, and X. Ma, "K2CO3-promoted methane pyrolysis on nickel/coal-char hybrids," *J Anal Appl Pyrolysis*, vol. 136, pp. 53–61, Nov. 2018, doi: 10.1016/J.JAAP.2018.11.001.

[99] N. Z. Muradov and T. N. Veziroğlu, "From hydrocarbon to hydrogen–carbon to hydrogen economy," *Int J Hydrogen Energy*, vol. 30, no. 3, pp. 225–237, Mar. 2005, doi: 10.1016/J.IJHYDENE.2004.03.033.

[100] H. F. Abbas and W. M. A. Wan Daud, "Hydrogen production by methane decomposition: A review," *Int J Hydrogen Energy*, vol. 35, no. 3, pp. 1160–1190, Feb. 2010, doi: 10.1016/J.IJHYDENE.2009.11.036.

[101] J. J. H. Togonon, P. C. Chiang, H. J. Lin, W. C. Tsai, and H. J. Yen, “Pure carbon-based electrodes for metal-ion batteries,” *Carbon Trends*, vol. 3, p. 100035, Apr. 2021, doi: 10.1016/J.CARTRE.2021.100035.

[102] T. J. Yokokura, Z. Qi, H. Wang, P. Manikandan, V. G. Pol, and J. R. Rodriguez, “Prolate carbon architecture as a novel Li-ion battery anode with kinetic study,” *Carbon Trends*, vol. 8, p. 100178, Jul. 2022, doi: 10.1016/J.CARTRE.2022.100178.

[103] F. Scala and P. Salatino, “Modelling fluidized bed combustion of high-volatile solid fuels,” *Chem Eng Sci*, vol. 57, no. 7, pp. 1175–1196, 2002, doi: 10.1016/S0009-2509(02)00004-0.

[104] B. Suleimenova, B. Aimbetov, D. Shah, E. J. Anthony, and Y. Sarbassov, “Attrition of high ash Ekibastuz coal in a bench scale fluidized bed rig under O2/N2 and O2/CO2 environments,” *Fuel Processing Technology*, vol. 216, Jun. 2021, doi: 10.1016/j.fuproc.2021.106775.

[105] D. K. Sarkar, “Fluidized-Bed Combustion Boilers,” D. K. B. T.-T. P. P. Sarkar, Ed., Elsevier, 2015, pp. 159–187. doi: https://doi.org/10.1016/B978-0-12-801575-9.00005-6.

[106] H. Zhang, K. Cen, J. Yan, and M. Ni, “The fragmentation of coal particles during the coal combustion in a fluidized bed,” *Fuel*, vol. 81, no. 14, pp. 1835–1840, 2002, doi: 10.1016/S0016-2361(02)00111-4.

[107] O. Senneca, M. Urciuolo, R. Chirone, and D. Cumbo, “An experimental study of fragmentation of coals during fast pyrolysis at high temperature and pressure,” *Fuel*, vol. 90, no. 9, pp. 2931–2938, 2011, doi: 10.1016/j.fuel.2011.04.012.

[108] M. Troiano, P. Ammendola, and F. Scala, “Attrition of lignite char under fluidized bed gasification conditions: The effect of carbon conversion,” *Proceedings of the Combustion Institute*, vol. 34, no. 2, pp. 2741–2747, 2013, doi: 10.1016/j.proci.2012.05.105.

[109] R. Chirone, L. Massimilla, and P. Salatino, “Comminution of carbons in fluidized bed combustion,” *Prog Energy Combust Sci*, vol. 17, no. 4, pp. 297–326, 1991, doi: 10.1016/0360-1285(91)90006-9.

[110] M. Kosowska-Galachowska and A. Luckos, “An experimental investigation into the fragmentation of coal particles in a fluidized-bed combustor,” *Proceedings of the 20th International Conference on Fluidized Bed Combustion*, no. 1991, pp. 330–334, 2009, doi: 10.1007/978-3-642-02682-9_47.

[111] D. Sasongko, C. B. Rasrendra, and A. Indarto, “Fragmentation model of coal devolatilisation in fluidised bed combustion,” *International Journal of Ambient Energy*, vol. 39, no. 5, pp. 508–515, 2018, doi: 10.1080/01430750.2017.1318788.

[112] P. Ammendola and F. Scala, “Attrition of lignite char during fluidized bed gasification,” *Exp Therm Fluid Sci*, vol. 43, pp. 9–12, 2012, doi: 10.1016/j.expthermflusci.2012.03.025.

[113] C. Pinho, “Fragmentation on batches of coke or char particles during fluidized bed combustion,” *Chemical Engineering Journal*, vol. 115, no. 3, pp. 147–155, 2006, doi: 10.1016/j.cej.2005.10.001.

[114] M. J. Paprika, M. S. Komatina, D. v. Dakić, and S. C. D. S. Nemoda, “Prediction of coal primary fragmentation and char particle size distribution in fluidized bed,” *Energy and Fuels*, vol. 27, no. 9, pp. 5488–5494, Sep. 2013, doi: 10.1021/ef400875q.

[115] Z. Ma, L. Cheng, L. Li, G. Luo, W. Zhang, and Y. Wu, "Pollutant emission and attrition performance of low calorific blended coals during co-combustion in fluidized bed," *Fuel*, vol. 331, Jan. 2023, doi: 10.1016/j.fuel.2022.125782.

[116] D. Li, Q. Deng, D. H. Lee, and C. hwan Jeon, "Prediction of attrition rate of coal ash for fluidized bed based on chemical composition with an artificial neural network model," *Fuel Processing Technology*, vol. 225, Jan. 2022, doi: 10.1016/j.fuproc.2021.107024.

[117] D. Müller, T. Plankenbühler, and J. Karl, "A Methodology for Measuring the Heat Release Efficiency in Bubbling Fluidised Bed Combustors," *Energies (Basel)*, vol. 13, no. 10, 2020, doi: 10.3390/en13102420.

[118] K. M. Merrett and K. J. Whitty, "Evaluation of coal conversion pathways in fluidized bed chemical looping combustion with oxygen uncoupling (CLOU)," *Fuel*, vol. 258, no. September, p. 116157, 2019, doi: 10.1016/j.fuel.2019.116157.

[119] F. Scala and R. Chirone, "Fluidized bed combustion of alternative solid fuels," *Exp Therm Fluid Sci*, vol. 28, no. 7, pp. 691–699, 2004, doi: 10.1016/j.expthermflusci.2003.12.005.

[120] M. Urciuolo, R. Solimene, R. Chirone, and P. Salatino, "Fluidized bed combustion and fragmentation of wet sewage sludge," *Exp Therm Fluid Sci*, vol. 43, pp. 97–104, 2012, doi: 10.1016/j.expthermflusci.2012.03.019.

[121] R. Chirone, P. Salatino, F. Scala, R. Solimene, and M. Urciuolo, "Fluidized bed combustion of pelletized biomass and waste-derived fuels," *Combust Flame*, vol. 155, no. 1–2, pp. 21–36, 2008, doi: 10.1016/j.combustflame.2008.05.013.

[122] F. Scala, R. Chirone, and P. Salatino, “Combustion and attrition of biomass chars in a fluidized bed,” *Energy and Fuels*, vol. 20, no. 1, pp. 91–102, 2006, doi: 10.1021/ef050102g.

[123] N. Jand and P. U. Foscolo, “Decomposition of wood particles in fluidized beds,” *Ind Eng Chem Res*, vol. 44, no. 14, pp. 5079–5089, 2005, doi: 10.1021/ie040170a.

[124] P. Ammendola, R. Chirone, G. Ruoppolo, and F. Scala, “The effect of pelletization on the attrition of wood under fluidized bed combustion and gasification conditions,” *Proceedings of the Combustion Institute*, vol. 34, no. 2, pp. 2735–2740, 2013, doi: 10.1016/j.proci.2012.06.008.

[125] C. C. Pereira and C. Pinho, “Influence of particle fragmentation and non-sphericity on the determination of diffusive and kinetic fluidized bed biochar combustion data,” *Fuel*, vol. 131, pp. 77–88, 2014, doi: 10.1016/j.fuel.2014.04.072.

[126] D. S. Litun, G. A. Ryabov, O. M. Folomeev, E. A. Shorina, and O. A. Smirnova, “Fragmentation and agglomeration of biomass in fluidised bed pyrolysis and combustion,” *J Phys Conf Ser*, vol. 1565, no. 1, 2020, doi: 10.1088/1742-6596/1565/1/012004.

[127] S. Wang *et al.*, “Mechanical strength evolution of biomass pellet during chemical looping gasification in fluidized bed,” *Fuel Processing Technology*, vol. 221, Oct. 2021, doi: 10.1016/j.fuproc.2021.106951.

[128] K. J. Timmer and R. C. Brown, “Transformation of char carbon during bubbling fluidized bed gasification of biomass,” *Fuel*, vol. 242, pp. 837–845, Apr. 2019, doi: 10.1016/j.fuel.2019.01.039.

[129] X. Yao, H. Zhang, H. Yang, Q. Liu, J. Wang, and G. Yue, “An experimental study on the primary fragmentation and attrition of limestones in a fluidized bed,” *Fuel Processing Technology*, vol. 91, no. 9, pp. 1119–1124, 2010, doi: 10.1016/j.fuproc.2010.03.025.

[130] F. Montagnaro, P. Salatino, and F. Scala, “The influence of temperature on limestone sulfation and attrition under fluidized bed combustion conditions,” *Exp Therm Fluid Sci*, vol. 34, no. 3, pp. 352–358, 2010, doi: 10.1016/j.expthermflusci.2009.10.013.

[131] M. Miao, B. Deng, X. Yao, G. Wei, M. Zhang, and H. Yang, “Experimental study on calcination and fragmentation characteristics of limestone in fluidized bed,” *Journal of the Energy Institute*, vol. 95, pp. 206–218, Apr. 2021, doi: 10.1016/j.joei.2021.01.014.

[132] M. Miao *et al.*, “Attrition performance and morphology of limestone under different conditions in fluidized bed,” *Fuel Processing Technology*, vol. 221, Oct. 2021, doi: 10.1016/j.fuproc.2021.106939.

[133] P. Basu, J. H. Greenblatt, and A. Basu, “Studies of the fragmentation of different coals in a fluidized bed,” *Journal of the Energy Institute*, vol. 78, no. 1, pp. 32–37, 2005, doi: 10.1179/174602205X39597.

[134] R. Chirone and L. Massimilla, “Primary Fragmentation of a Coal in Fluidized Bed Combustion,” *Twenty-Second Symposium (International) on Combustion*, vol. 24, pp. 267–277, 1988.

[135] P. M. Walsh and T. Li, “Fragmentation and attrition of coal char particles undergoing collisions during combustion at temperatures from 900 to 1100 K,” *Combust Flame*, vol. 99, no. 3–4, pp. 749–757, 1994, doi: 10.1016/0010-2180(94)90070-1.

[136] K. S. Pragadeesh, I. Regupathi, and D. Ruben Sudhakar, “Insitu gasification – chemical looping combustion of large coal and biomass particles: Char conversion and comminution,” *Fuel*, vol. 292, no. February, p. 120201, 2021, doi: 10.1016/j.fuel.2021.120201.

[137] D. S. Litun and G. A. Ryabov, “Modern State and Topical Issues of Studying Solid Fuel Particle Primary Fragmentation Processes as Applied to Biomass Combustion and Gasification in Fluidized and Dense Bed (Review),” *Thermal Engineering* , vol. 65, no. 12, pp. 875–884, Dec. 2018, doi: 10.1134/S0040601518120042.

[138] D. Litoun, G. Ryabov, and A. Pchelincev, “Fragmentation of biomass particles in fixed and fluidized bed combustion and gasification,” in *Journal of Physics: Conference Series*, Institute of Physics Publishing, Jun. 2019. doi: 10.1088/1742-6596/1261/1/012021.

[139] D. S. Litun, G. A. Ryabov, and E. A. Shorina, “Features of Primary Fragmentation of Wood Biomass during Fast Heating and Devolatilization,” *Thermal Engineering* , vol. 69, no. 7, pp. 523–534, Jul. 2022, doi: 10.1134/S0040601522070035.

[140] O. Senneca, M. Urciuolo, and R. Chirone, “A semidetailed model of primary fragmentation of coal,” *Fuel*, vol. 104, pp. 253–261, Feb. 2013, doi: 10.1016/j.fuel.2012.09.026.

[141] F. Scala, P. Salatino, and R. Chirone, “Fluidized Bed Combustion of a Biomass Char (Robinia pseudoacacia),” *Energy & Fuels*, vol. 76, no. 4, pp. 1058–1067, 2000.

[142] D. Yan, M. Li, L. Zou, M. Gu, M. Li, and F. Wang, “A study on fragmentation and emissions characteristics during combustion of injected pulverizcred coal,” *Fuel*, vol. 309, Feb. 2022, doi: 10.1016/j.fuel.2021.122152.

[143] S. Zhong, H. Yue, F. Baitalow, M. Reinmöller, and B. Meyer, “In-situ investigation of coal particle fragmentation induced by thermal stress and numerical analysis of the main influencing factors,” *Energy*, vol. 215, Jan. 2021, doi: 10.1016/j.energy.2020.119138.

[144] P. Ammendola, R. Chirone, F. Miccio, G. Ruoppolo, and F. Scala, “Devolatilization and attrition behavior of fuel pellets during fluidized-bed gasification,” *Energy and Fuels*, vol. 25, no. 3, pp. 1260–1266, 2011, doi: 10.1021/ef101614j.

[145] J. M. Lee, J. S. Kim, and J. J. Kim, “Comminution characteristics of Korean anthracite in a CFB reactor,” *Fuel*, vol. 82, no. 11, pp. 1349–1357, 2003, doi: 10.1016/S0016-2361(03)00022-X.

[146] D. Dakič, G. van der Honing, and M. Valk, “Fragmentation and swelling of various coals during devolatilization in a fluidized bed,” *Fuel*, vol. 68, no. 7, pp. 911–916, 1989, doi: 10.1016/0016-2361(89)90129-4.

[147] S. Zhong, F. Baitalow, and B. Meyer, “Experimental investigation on fragmentation initiation of mm-sized coal particles in a drop-tube furnace,” *Fuel*, vol. 234, no. June, pp. 473–481, 2018, doi: 10.1016/j.fuel.2018.06.059.

[148] H. Wang *et al.*, “Primary Fragmentation Characteristics in the Process of Coal Slime Combustion,” *Combustion Science and Technology*, vol. 00, no. 00, pp. 1–18, 2021, doi: 10.1080/00102202.2021.1998822.

[149] M. Kosowska-Golachowska, “Coal Combustion,” in *Structure and Reactivity of Coal*, vol. 4, 2015, pp. 269–304. doi: 10.1007/978-3-662-47337-5_7.

[150] U. Arena, A. Cammarota, and R. Chirone, “Primary and secondary fragmentation of coals in a circulating fluidized bed combustor,” *Symposium (International) on Combustion*, vol. 25, no. 1, pp. 219–226, 1994, doi: 10.1016/S0082-0784(06)80647-8.

[151] P. Dacombe, M. Pourkashanian, A. Williams, and L. Yap, “Combustion-induced fragmentation behavior of isolated coal particles.” [Online]. Available: www.elsevier.com/locate/fuel

[152] T. Cui, Z. Zhou, Z. Dai, C. Li, G. Yu, and F. Wang, “Primary Fragmentation Characteristics of Coal Particles during Rapid Pyrolysis,” *Energy and Fuels*, vol. 29, no. 10, pp. 6231–6241, Oct. 2015, doi: 10.1021/acs.energyfuels.5b01289.

[153] A. Blaszczuk and W. Nowak, “Bed-to-wall heat transfer coefficient in a supercritical CFB boiler at different bed particle sizes,” *Int J Heat Mass Transf*, vol. 79, pp. 736–749, 2014, doi: 10.1016/j.ijheatmasstransfer.2014.08.080.

[154] L. Chen, C. Dupont, S. Salvador, M. Grateau, G. Boissonnet, and D. Schweich, “Experimental study on fast pyrolysis of free-falling millimetric biomass particles between 800 °C and 1000 °C,” *Fuel*, vol. 106, pp. 61–66, 2013, doi: 10.1016/j.fuel.2012.11.058.

[155] M. J. Paprika, M. S. Komatina, D. v. Dakić, and S. C. D. S. Nemoda, “Prediction of coal primary fragmentation and char particle size distribution in fluidized bed,” *Energy and Fuels*, vol. 27, no. 9, pp. 5488–5494, Sep. 2013, doi: 10.1021/ef400875q.